

# ÅBO AKADEMI

FAKULTETEN FÖR  
NATURVETENSKAPER OCH  
TEKNIK

FACULTY OF  
SCIENCE AND  
ENGINEERING

Johan Gadolin  
processkemiska centret

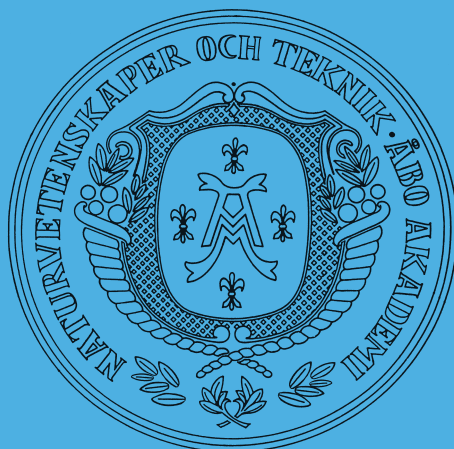
Johan Gadolin  
Process Chemistry Centre

---

## REPORT 16-02

Chemistry of potassium halides and their role in  
corrosion in biomass and waste firing

Hao Wu



**Doctoral Thesis**

**Laboratory of Inorganic Chemistry**

# Chemistry of potassium halides and their role in corrosion in biomass and waste firing

Hao Wu



## Doctoral Thesis

Laboratory of Inorganic Chemistry  
Department of Chemical Engineering  
Johan Gadolin Process Chemistry Center  
Åbo Akademi University  
Turku/Åbo, Finland, 2016

## **Supervisors**

Docent Patrik Yrjas  
Åbo Akademi University

Professor Mikko Hupa  
Åbo Akademi University

## **Opponent**

Professor Rainer Backman  
Umeå University

## **Reviewers**

Docent Minna Tiainen  
University of Oulu

D.Sc. Markus Broström  
Umeå University

ISSN 2343-2535  
ISBN 978-952-12-3400-2 (printed edition)  
ISBN 978-952-12-3401-9 (digital edition)  
Painosalama Oy  
Åbo, Finland, 2016

## **Preface**

This work was carried out at the Laboratory of Inorganic Chemistry at the Department of Chemical Engineering at Åbo Akademi University. The research has been carried out within the projects FUSEC (2011–2014) and CLIFF (2014–2017) as part of the activities of the Åbo Akademi Johan Gadolin Process Chemistry Centre. These projects were financially supported by the National Technology Agency of Finland (Tekes), Andritz Oy, Valmet Technologies Oy, Amec Foster Wheeler Energia Oy, UPM-Kymmene Oyj, Clyde Bergemann GmbH, International Paper Inc., and Top Analytica Oy Ab. Other research partners are VTT, Lappeenranta University of Technology, Aalto University and Tampere University of Technology. Financial support has also been obtained from the Åbo Akademi Rector Scholarship, the RECOMBIO EU-project TREN/FP7EN/239530/ and the Academy of Finland project “Chemistry of biomass impurities at reducing conditions in future thermal conversion concepts” (Decision no. 269277). All financial support is gratefully acknowledged.

I would like to express my deepest gratitude to my supervisors, Docent Patrik Yrjas and Professor Mikko Hupa for their great support, encouragement and guidance during my doctoral studies. Without both of you the thesis work could not have been possible. I am very grateful to Professor Mikko Hupa, the rector of Åbo Akademi University, who gave me the opportunity to study in his group. Despite he has really tight schedule he always had time to answer my questions. I appreciate all the discussions we have had. I wish to express my deepest thanks to my day-to-day supervisor Docent Patrik Yrjas for his trust and his great patience. The PhD study is very hard for me, a lot of painful struggling. Patrik, thank you for helping me grow in confidence and taking good care of me. Thank you for all the tremendous help and inspiration you gave me both in the research and writing work and in my life.

I wish to thank all of my co-authors for their contributions to this work. Particularly D.Sc. Dorota Bankiewicz, thank you for your great help and supervision at the most critical moments, sharing your experience on corrosion, good suggestion and comments in the experimental, results and paper writing. Also, thank you for your care and encouragement inside and outside the research work. D.Sc. Pasi Vainikka, especially thank you for giving me the opportunity to work with VTT

## *Preface*

---

to perform the bench-scale campaigns and providing the invaluable industrial experience and your expertise on bromine research. Also, thank you for the great support and inspiration you gave me, and the helpful ideas about the test plan and results evaluation. Lic.Sc. Tor Laurén, thank you for your great help in results and discussion and sharing your experience with me. D.Sc. Daniel Lindberg, thank you for your help in thermodynamic calculations which strongly support the experimental results.

I am grateful to Marko Räsänen, Juho Kauppinen and Raili Taipale for their help in performing the experiments at VTT.

I wish to express my sincere gratitude to Professor Leena Hupa for her support in the last year of the thesis work. I want to thank Mr. Linus Silvander for his invaluable work in SEM/EDX analysis. Great thanks to Ms. Jaana Paananen for her laboratory support and help. I wish to thank Lic.Sc. Micaela Westèn for teaching me the corrosion test method, which I used in this work.

I would like to thank all the colleagues of the Laboratory of Inorganic Chemistry for a pleasant work atmosphere and for their kind help. I feel very lucky to be a member of our group.

I am also grateful to Professor Menghua Qin and Professor Huayu Qiu for suggesting Finland as a country in which I could continue my studies.

I would like to thank all my friends for the happiness and enjoyment these years! Thank you for your help, encouragement, and being together to laugh and to cry.

Finally, I would like to thank my dear mother and father! Thank you for your love, support and encouragement during my studies and my life. I love you!

Åbo, March 2016

Hao Wu

## **Abstract**

Compared to the use of traditional fossil fuels (coal, oil, natural gas), combustion of biomass and waste fuels has several environmental and economic advantages for heat and power generation. However, biomass and waste fuels might contain halogens (Cl, Br, F), alkali metals (Na, K) and heavy metals (Zn, Pb), which may cause harmful emissions and corrosion problems. High-temperature corrosion occurs typically on furnace waterwalls and superheaters. The corrosion of the boiler tube materials limits the increase of thermal efficiency of steam boilers and leads to costly shutdowns and repairs.

In recent years, some concerns have been raised about halogen (Cl, Br, and F)-related high-temperature corrosion in biomass- and waste-fired boilers. Chlorine-related high-temperature corrosion has been studied extensively. The presence of alkali chlorides in the deposits is believed to play a major role in the corrosion observed in biomass and waste fired boilers. However, there is much less information found in literature on the corrosion effect of bromine and fluorine. According to the literature, bromine is only assumed to play a role similar to chlorine; the role of fluorine is even less understood.

In this work, a series of bubbling fluidized bed (BFB) bench-scale tests were carried out to characterize the formation and sulfation behaviors of KCl and KBr in BFB combustion conditions. Furthermore, a series of laboratory tests were carried out to investigate the high-temperature corrosion behaviors of three different superheater steels (10CrMo9-10, AISI 347 and Sanicro 28) exposed to potassium halides in ambient air and wet air (containing 30% H<sub>2</sub>O). The influence of H<sub>2</sub>O and O<sub>2</sub> on the high-temperature corrosion of steels both with and without a salt (KCl) in three gas atmospheres (2% H<sub>2</sub>O-30% O<sub>2</sub>-N<sub>2</sub>, 2% H<sub>2</sub>O-2% O<sub>2</sub>-N<sub>2</sub> and 30% H<sub>2</sub>O-2% O<sub>2</sub>-N<sub>2</sub>) was also studied.

From the bench-scale BFB combustion tests, it was found that HBr has a clearly higher affinity for the available K forming KBr than HCl forming KCl. The tests also indicated that KCl has a higher tendency for sulfation than KBr.

## *Abstract*

---

From the laboratory corrosion tests in ambient air (also called “dry air” in **Paper III** and **Paper IV**), it was found that at relatively low temperatures ( $\leq 550$  °C) the corrosivity of KBr and KF are similar to KCl. At 600 °C, KF showed much stronger corrosivity than KBr and KCl, especially for 10CrMo9-10 and AISI 347. When exposed to KBr or KF, 10CrMo9-10 was durable at least up to 450 °C, while AISI 347 and Sanicro 28 were durable at least up to 550 °C.

From the laboratory corrosion tests in wet air (30% H<sub>2</sub>O), no obvious effect of water vapor was detected at 450 °C. At 550 °C, the influence of water vapor became significant in some cases, but the trend was not consistent. At 550 °C, after exposure with KBr, 10CrMo9-10 suffered from extreme corrosion; after exposure with KF and KCl, the corrosion was less severe, but still high. At 550 °C, local deep pitting corrosion occurred on AISI 347 and Sanicro 28 after exposure with KF. Some formation of K<sub>2</sub>CrO<sub>4</sub> was observed in the oxide layer. At 550 °C, AISI 347 and Sanicro 28 suffered from low corrosion (oxide layer thickness of  $< 10$   $\mu\text{m}$ ) after exposure with KBr and KCl. No formation of K<sub>2</sub>CrO<sub>4</sub> was observed. Internal oxidation occurred in the cases of AISI 347 with KBr and KCl.

From the laboratory corrosion tests in three different gas atmospheres (2% H<sub>2</sub>O-30% O<sub>2</sub>-N<sub>2</sub>, 2% H<sub>2</sub>O-2% O<sub>2</sub>-N<sub>2</sub> and 30% H<sub>2</sub>O-2% O<sub>2</sub>-N<sub>2</sub>), it was found that in tests with no salt, no corrosion occurred on AISI 347 and Sanicro 28 up to 600 °C in both the “O<sub>2</sub>-rich” (2% H<sub>2</sub>O-30% O<sub>2</sub>-N<sub>2</sub>) and “H<sub>2</sub>O-rich” (30% H<sub>2</sub>O-2% O<sub>2</sub>-N<sub>2</sub>) gas atmospheres; only 10CrMo9-10 showed increased corrosion with increasing temperature. For 10CrMo9-10 in the “O<sub>2</sub>-rich” atmosphere, the presence of KCl significantly increased the corrosion compared to the “no salt” cases. For 10CrMo9-10 in the “H<sub>2</sub>O-rich” atmosphere, the presence or absence of KCl did not show any big influence on corrosion. The formation of K<sub>2</sub>CrO<sub>4</sub> was observed only in the case with the “O<sub>2</sub>-rich” atmosphere.

Considering both the results from the BFB tests and the laboratory corrosion tests, if fuels containing Br were to be combusted, the corrosion damage of superheaters would be expected to be higher than if the fuels contain only Cl. Information generated from these studies can be used to help the boiler manufacturers in selecting materials for the most demanding combustion systems.

## **Svensk sammanfattning (Summary in Swedish)**

I jämförelse med användandet av traditionella fossila bränslen, (kol, olja, naturgas) har förbränning av biobränslen och avfall många fördelaktiga effekter på miljön, och ger dessutom möjligheter till ekonomiska fördelar vid produktion av värme och elektricitet. Biobränslen och avfall kan emellertid innehålla halogener (Cl, Br, F), alkalimetaller (Na, K), och tungmetaller (Zn, Pb) som kan förorsaka skadliga utsläpp och korrosionsproblem. Högtemperaturkorrosion förekommer typiskt på pannväggar och överhettarrör. Korrosion på pannors överhettarrör begränsar det maximala utnyttjandet av pannans termiska kapacitet och förorsakar även kostsamma driftstopp och reparationer.

På senare tid har korrosion vid höga temperaturer, där halogener (Cl, Br och F) spelar en stor roll, börjat uppmärksammas i pannor som eldas med biobränslen och avfall. Högtemperaturkorrosion relaterad till klor (Cl) har undersökts grundligt. Närvaron av alkaliklorider i beläggningar från pannor som eldas med biobränslen och avfall anses ha en stor betydelse för korrosionen. Den publicerade informationen, som beskriver hur brom och fluor påverkar korrosionen, är emellertid relativt begränsad. Enligt tillgänglig information antas brom spela samma roll som klor i korrosionsförloppet. Fluors betydelse i sammanhanget är ännu sämre klagjord.

I detta arbete har en serie experiment i en experimentell testanläggning, en s.k. bubblande fluidiserad bädd (BFB), utförts, för att karaktärisera bildnings- och sulfateringsbeteendet hos KCl och KBr. Dessutom har tre olika ståls korrosionsbeteende vid höga temperaturer undersökts. Stålsprov (10CrMo9-10, AISI 347 och Sanicro 28) av samma kvalitet som används i existerande pannors överhettarrör, utsattes för kaliumhalider i laboratorieförsök i normalatmosfär och i normalatmosfär innehållande 30% vattenånga. Vattenångans och syrets inverkan på stålens högtemperaturkorrosion, både i närvaro och i frånvaro av ett salt (KCl), undersöktes i tre olika gasatmosfärer (2% H<sub>2</sub>O-30% O<sub>2</sub>-N<sub>2</sub>, 2% H<sub>2</sub>O-2% O<sub>2</sub>-N<sub>2</sub> och 30% H<sub>2</sub>O-2% O<sub>2</sub>-N<sub>2</sub>).

Resultaten från BFB-försöken visade att HBr har en högre affinitet gentemot den tillgängliga kaliumbildande kaliumbromiden än gentemot den HCl-bildande kaliumkloriden. Experimenten visade även att kaliumklorid har en tendens att lättare sulfateras än kaliumbromid.



## *Svensk sammanfattning (Summary in Swedish)*

---

Från korrosionstesten, gjorda i normalatmosfär i laboratorieförhållanden, (kallas även "torr luft" i publikationerna Paper III och Paper IV) kan noteras att vid relativt låga temperaturer ( $\leq 550$  °C) är korrosionsbenägenheten för KBr och KF densamma som för KCl. Vid 600 °C, bidrog KF i högre utsträckning till korrosion än KBr och KCl, speciellt på 10CrMo9-10 och AISI 347. När 10CrMo9-10 utsattes för KBr och KCl var provet beständigt åtminstone upp till 450 °C, medan AISI 347 och Sanicro 28 visade beständighet upp till åtminstone 550 °C.

Laboratoriekorrosionsexperiment gjorda i normalatmosfär med vattenånga (30% H<sub>2</sub>O), påvisade ingen effekt av vattenångans närvaro vid 450 °C. Vid 550 °C kunde en tydlig effekt av vattenångans närvaro ses i en del fall, även om trenden var inkonsekvent. Vid 550 °C då 10CrMo9-10 utsattes för KBr blev korrosionen kraftig, medan då samma material utsattes för KF och KCl blev korrosionen mindre påtaglig, men dock fortfarande tydlig. Vid 550 °C uppträdde lokal gropfrätning på AISI 347 och Sanicro 28 efter att de utsattes för KF. En blygsam bildning av K<sub>2</sub>CrO<sub>4</sub> kunde observeras i oxidskiktet. Vid 550 °C förorsakades svag korrosion på AISI 347 och Sanicro 28 (oxidlagrets tjocklek < 10 µm) efter att de utsattes för KBr and KCl. Ingen bildning av K<sub>2</sub>CrO<sub>4</sub> observerades. Intern oxidering skedde då AISI 347 utsattes för KBr och KCl.

När laboratorieexperiment utfördes i tre olika gasatmosfärer (2% H<sub>2</sub>O-30% O<sub>2</sub>-N<sub>2</sub>, 2% H<sub>2</sub>O-2% O<sub>2</sub>-N<sub>2</sub> och 30% H<sub>2</sub>O-2% O<sub>2</sub>-N<sub>2</sub>) utan salt med AISI 347 och Sanicro 28 kunde ingen korrosion observeras även vid 600 °C. Endast 10CrMo9-10 uppvisade en tilltagande korrosion med stigande temperatur. I fallet med 10CrMo9-10 i syrerik atmosfär och, med KCl närvarande, ökade korrosionsangreppet märkbart jämfört med fallet utan salt. För 10CrMo9-10, i vattenrik gasatmosfär, kunde ingen större skillnad observeras mellan fallen med eller utan KCl. Bildandet av K<sub>2</sub>CrO<sub>4</sub> observerades endast i fallet med syrerik atmosfär.

Med beaktande av resultaten från både BFB-testen och korrosionstesten gjorda i laboratoriet kan man dra slutsatsen, att om avsikten är att bränna bränslen innehållande Br, kan korrosionsskadorna på överhettarna förväntas bli större, än om bränslet enbart skulle innehålla Cl. De rön, som uppbringats genom studierna, som beskrivs i denna avhandling, kan hjälpa pannstillverkarna att välja material vid byggandet av de mest krävande förbränningsanläggningarna.

## List of publications

This thesis is based on the following papers:

- I. Fate of bromine and chlorine in bubbling fluidized bed combustion – Formation of alkali halide aerosols  
Wu H., Laurén T., Yrjas P., Vainikka P., Hupa M. **Fuel** 128 (2014) 390-395.
  
- II. Sulfation of alkali halides in a bench-scale bubbling fluidized bed reactor  
Wu H., Yrjas P., Vainikka P., Lindberg D., Hupa M. **Fuel** 177 (2016) 173–179.
  
- III. Laboratory studies of potassium-halide-induced high-temperature corrosion of superheater steels. Part 1: exposures in dry air  
Wu H., Yrjas P., Hupa M. **Energy & Fuels**, 29 (2015) 1186-1195.
  
- IV. Laboratory studies of potassium-halide-induced high-temperature corrosion of superheater steels. Part 2: exposures in wet air  
Wu H., Bankiewicz D., Yrjas P., Hupa M. **Energy & Fuels** 29 (2015) 2709-2718.
  
- V. The influence of H<sub>2</sub>O/O<sub>2</sub> ratios on high-temperature corrosion of superheater steels  
Wu H., Bankiewicz D., Yrjas P., Lindberg D., Hupa M. Submitted on April 16, 2016 to **Corrosion Science**.

## **Author's contribution**

### **Paper I.**

Wu H. designed the test matrix together with the co-authors, participated and followed the tests, and evaluated the results. The operation of the bench-scale boiler and the surrounding equipment in the tests was done by VTT operators. She was principally responsible for writing the paper.

### **Paper II.**

Wu H. designed the test matrix together with the co-authors, participated and followed the tests, and evaluated the results. The operation of the bench-scale boiler and the surrounding equipment in the tests was done by VTT operators. Lindberg D. performed the thermodynamic calculations. Wu H. was principally responsible for writing the paper.

### **Paper III.**

Wu H. designed the test matrix together with the co-authors, performed the tests, and evaluated the results. She was principally responsible for writing the paper.

### **Paper IV.**

Wu H. designed the test matrix together with the co-authors, performed the tests, and evaluated the results. She was principally responsible for writing the paper.

### **Paper V**

Wu H. together with the co-authors designed the test matrix, performed the tests, and evaluated the results. Lindberg D. performed the thermodynamic calculations. Wu H. was responsible for the paper. Wu H. and Bankiewicz D. were the main writers of the paper.

## **Related publications not included in the thesis:**

Fate of bromine and chlorine in bubbling fluidized bed combustion – formation of alkali halide aerosols

Wu H., Laurén T., Yrjas P., Vainikka P., Hupa M. **Impacts of Fuel Quality on Power Production and Environment**, September 23-27, 2012, Puchberg am Schneeberg, Austria. Conference Proceedings.

Alkali-chloride and -bromide aerosol formation and corrosion in biomass and waste firing conditions

Wu H., Laurén T., Yrjas P., Vainikka P., Hupa M. **The 18th IFRF Members' Conference – Flexible and clean fuel conversion in industry**, June 1-3, 2015, Freising, Germany. Conference Proceedings.

## **Table of contents**

*Preface*

*Abstract*

*Svensk sammanfattning (Summary in Swedish)*

*List of publications*

*Author's contribution*

### **Table of contents**

<b>1. INTRODUCTION.....</b>	<b>1 -</b>
<b>2. BACKGROUND.....</b>	<b>2 -</b>
<b>2.1 Fluidized bed boilers.....</b>	<b>2 -</b>
2.1.1 Bubbling Fluidized bed (BFB) boiler .....	3 -
<b>2.2 Biomass and waste fuels.....</b>	<b>5 -</b>
<b>2.3 Sources of halogens (F, Cl, Br) in waste fuels.....</b>	<b>7 -</b>
<b>2.4 Release of ash-forming matter .....</b>	<b>10 -</b>
<b>2.5 Release of halogens.....</b>	<b>12 -</b>
<b>2.6 Alkali chloride-induced corrosion .....</b>	<b>13 -</b>
<b>2.7 Bromine- or fluorine-induced corrosion .....</b>	<b>14 -</b>
<b>2.8 The effect of water vapor on high-temperature corrosion .....</b>	<b>16 -</b>
<b>2.9 Sulfation of alkali chlorides.....</b>	<b>17 -</b>
<b>3. EXPERIMENTAL .....</b>	<b>18 -</b>

## *Table of contents*

---

<b>3.1 Bench-scale BFB tests .....</b>	<b>- 18 -</b>
3.1.1 The bench-scale BFB reactor .....	- 19 -
3.1.2 Flue gas analysis.....	- 20 -
3.1.3 Aerosol sampling .....	- 21 -
3.1.4 Deposit sampling .....	- 23 -
<b>3.2 Laboratory-scale high-temperature corrosion tests .....</b>	<b>- 24 -</b>
<b>4. RESULTS AND DISCUSSION .....</b>	<b>- 25 -</b>
<b>4.1 BFB test results.....</b>	<b>- 25 -</b>
4.1.1 Formation of alkali halides (Paper I).....	- 25 -
4.1.2 Sulfation of alkali halides (Paper II) .....	- 28 -
<b>4.2 Laboratory corrosion test results .....</b>	<b>- 29 -</b>
4.2.1 Potassium halide-induced corrosion in dry conditions (Paper III).....	- 29 -
4.2.2 Potassium halide-induced corrosion in wet conditions (Paper IV).....	- 34 -
4.2.3 Comparison the corrosion behavior in dry and wet conditions (Papers III and IV) .....	- 35 -
4.2.4 The influence of H <sub>2</sub> O/O <sub>2</sub> ratios on KCl-induced corrosion (Paper V) .....	- 44 -
<b>5. CONCLUSIONS .....</b>	<b>- 49 -</b>
<b>REFERENCES.....</b>	<b>- 52 -</b>



# 1. INTRODUCTION

Combustion of biomass and waste for heat and power generation, compared to fossil fuels, is a technically feasible option for the reduction of CO<sub>2</sub>-emissions. However, combustion of biomass and waste often leads to high-temperature corrosion problems. High-temperature corrosion occurs typically on furnace waterwalls and superheaters. The corrosion of boiler tube materials limits the increase of thermal efficiency of biomass- and waste-fired boilers and leads to costly shutdowns and repairs.

In recent years, some concerns about halogen (Cl, Br, and F)-related high-temperature corrosion in biomass- and waste-fired boilers have been raised. Chlorine-related high-temperature corrosion has been widely studied. The presence of alkali chlorides in the deposits is believed to play a major role in the corrosion observed in biomass- and waste-fired boilers [1-7]. Chlorine in waste fuels originates mainly from chlorinated plastics, e.g., polyvinyl chloride (PVC), or food residues containing dietary salt, e.g., sodium chloride (NaCl) [3, 8, 9]. Much less information concerning bromine and fluorine induced high-temperature corrosion is available if compared to chlorine. Bromine is assumed to play a similar role as chlorine [10-15], while the role of fluorine is even less understood. The main reason behind this lack of knowledge is the relatively low concentrations of Br and F in biomass and waste fuels. However, the Br concentration can occasionally be much higher if the waste fuels are rich in flame-retarded plastics and textiles [11, 16, 17], while F may enter the combustion system along with special plastics and textiles containing fluoropolymers and other fluorinated organic compounds [18].

### *Main Objectives*

The purpose of this work was to shed more light on the role and behavior of bromine and fluorine in combustion of biomass or waste derived fuels, and to find ways to control or avoid problems caused by alkali halides especially high-temperature corrosion. In particular, the following topics were studied:



## **2. BACKGROUND**

---

- formation and sulfation of alkali halides in BFB combustion conditions, especially comparisons between KCl and KBr
- KBr- and KF-induced high-temperature corrosion under dry and wet conditions
- the effect of water vapor on high-temperature corrosion, especially the influence of H<sub>2</sub>O/O<sub>2</sub> ratios on KCl-induced corrosion

## **2. BACKGROUND**

### **2.1 Fluidized bed boilers**

In the 1970s, fluidized bed combustion technology was first applied for large-scale power production from burning solid fuels. Nowadays the fluidized bed technology has become one of the most common combustion technologies for heat and electricity generation from biomass and waste fuels. The fluidized bed combustion technology can cope with a wide range of fuels (varying in the ash content, moisture content or heating value) and variable fuel mixtures.

In a fluidized bed boiler, a continuous upward stream of air (the primary air or fluidizing air) enters from the bottom of the bed, and the fuel is burnt in a suspension of gas and solid bed materials (usually sand). The turbulent mixing of gas and bed particles behaves like a boiling liquid. Also the good mixing of fuel and bed particles provides effective heat transfer, which results in high combustion efficiencies and low emissions.

In terms of the fluidizing air velocity, fluidized bed boilers can be divided into two groups: circulating fluidized bed (CFB) boilers and bubbling fluidized bed (BFB) boilers. In a CFB boiler, the air velocity is sufficiently high (4-9 m/s), so that the bed particles are entrained with the flue gas stream, separated in a cyclone, and then recirculated back to the bed. In a BFB boiler, the air velocity is lower (1-4 m/s), and thus the bed particles remain suspended in the bottom part of the furnace.

The choice between BFB and CFB combustion technology is largely linked to the fuel qualities and the size of the boiler. BFB boilers are more suited for biomass or low-grade fuels with low

## 2. BACKGROUND

---

heating value and high moisture content, such as sludge and bark. CFB boilers are commonly used for fuels with high heating value, such as coal and recovered fuel (REF). For reactive fuels such as wood, wood waste or peat, both types of boilers are applicable. For less reactive fuels such as coal, CFB boilers are preferred [19]. BFB boilers are rather small in size, normally ranging from 15-50 MWth, but there are also larger units close to 300 MWth. CFB boilers are mostly favored in larger-scale applications (up to several 100 MWth) [6].

The following chapter gives a brief description of the BFB boiler, since this type of technology was utilized in two experimental studies performed in this work (**Papers I & II**).

### 2.1.1 Bubbling Fluidized bed (BFB) boiler

A BFB boiler can generally be divided into three main sections: the lower furnace, the freeboard and the convective section (superheaters, economizers and air preheaters). A schematic picture of a typical BFB boiler is shown in Figure 1. At the bottom of the furnace, fuel is added onto a bed of inert particles (e.g., sand). The fluidizing air (primary air) is fed from below through air nozzles into the bed. At a suitable air velocity, bubbles of air start to form, and the bed becomes fluidized. In the bed, fuel drying, volatilization, ignition and combustion take place. Such turbulent and constant mixing of fuel and bed particles provides effective heat transfer and good combustion. The bed temperature is generally kept around 750-900 °C; at lower temperatures the combustion cannot be sustained, and at higher temperatures bed sintering may occur [6]. The walls of the lower furnace are covered with refractory materials, which minimize heat loss from the bed and protect the wall tubes from erosion.

## 2. BACKGROUND

---

**E.ON UK, Steven's Croft Power Station, Lockerbie, UK**  
Steam 126 MW<sub>th</sub> - 48 kg/s - 137 bar - 537 °C  
Fuels Wood chips, sawdust, bark, recycled wood  
Start-up 2007

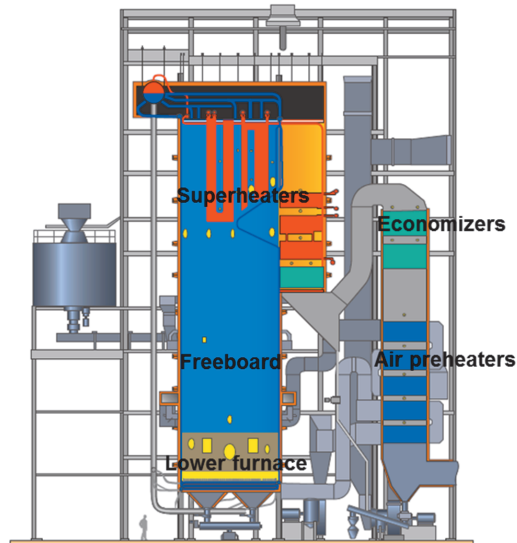


Figure 1. A schematic picture of a BFB boiler (Courtesy of Valmet Technologies Oy).

Combustion takes place mostly in the bed and partly in the freeboard above the bed. The flue gases carry finer particles leaving the bed, and pass through the freeboard region. Additional air (secondary and tertiary air) is fed into the freeboard to complete the combustion. Thereby some smaller char particles and volatiles could continue to burn in the freeboard. The furnace temperature in the BFB boiler depends on the moisture content of fuel and air distribution. Typically, the highest temperature, about 1000-1300 °C, is achieved at the secondary air level. The furnace walls consist of evaporator tubes forming membrane waterwalls. In the waterwall tubes, water is turned into steam by the heat generated from combustion.

After exiting the combustion zone, the flue gases pass through the convective section, where heat is further recovered and flue gases are cooled down. The convective section typically includes primary, secondary and tertiary superheaters, economizers and air preheaters. The secondary and tertiary superheaters are the hottest, and thus most susceptible to high-temperature corrosion. The

## **2. BACKGROUND**

---

typical temperature of flue gas entering the superheater region is about 900-1000 °C. The flue gases and material temperatures at the economizers and air preheaters are much lower, but the conditions are often still corrosive [20].

The flue gases leave the convective section, and then pass through a particulate control device, such as cyclone, bag filter or electrostatic precipitator. The flue gases may in some cases still be cleaned from gaseous pollutants by e.g. a scrubber. Finally, the cleaned flue gases are discharged into the atmosphere through a stack.

### **2.2 Biomass and waste fuels**

Biomass is a biological organic material derived from various living organisms. Biomass can be used as a source of energy via different thermal (e.g., combustion, pyrolysis or gasification), chemical, biochemical or electrochemical methods. The common biomass fuels used in power generation are wood (including forest residues), bark, agricultural residues, straw, black liquor, sewage sludge and wood waste. The renewability, diversity and potential CO<sub>2</sub>-neutrality of biomass make it a feasible alternative to fossil fuels for future energy demand.

Biomass has a different chemical composition and different combustion characteristics than fossil fuels. Generally, biomass fuels have higher volatile and moisture contents, lower sulfur and char contents than coal. Elements such as K, Cl and S in biomass largely volatilize during combustion and form fine particles [21-24]. The heating values of biomass fuels are generally much lower than those of fossil fuels. Consequently, the combustion temperatures of biomass are usually significantly lower than those of fossil fuels. Table 1 shows typical properties of some biomass fuels.

## 2. BACKGROUND

Table 1. Average properties of some biomass fuels. (Source: [6])

	Wood	Pulp mill sludge	Straw	Bark	Black liquor
<b>Moisture (%)</b>	10-40	60-85	8-16	45-65	15-35
<b>Ash (% in ds)</b>	1-10	5-35	3-12	2-10	40-45
<b>LHV (MJ/kg ar)</b>	10-18	0-6	12-16	4-10	11-13 <sup>a</sup>
<b>S (% in ds)</b>	0.03-0.15	0.4-1.7	0.05-0.17	0.03-0.1	3-8
<b>Cl (% in ds)</b>	0.01-0.04	0.04-0.3	0.01-1.5	0-0.3	0.2-2.5
<b>Na (% in ash)</b>	0.3-0.8	0.1-3.3	0.06-2.2	0.1-1.2	19-23 <sup>a</sup>
<b>K (% in ash)</b>	3-8	0.2-2.0	5-32	1-4	0.1-8 <sup>a</sup>
<b>Ca(% in ash)</b>	5-40	6-50	2-13	16-32	-

<sup>a</sup> in black liquor dry solids

According to EuroStat and relevant European Union directives [25-27], anthropogenic wastes are classified in different groups. Vainikka [28] summarized the common used denotations:

- HHW: Household Waste. With or without source separation.
- CIW: Commercial and Industrial Waste. Typically packaging and other types of waste from commerce, offices, and public buildings collected in a similar way as HHW.
- MSW: Municipal Solid Waste = HHW + CIW [29].
- SRF: Solid Recovered Fuel. Fuels classified and certified according to CEN-TC 343 [30, 31]. SRF can be prepared from HHW and/or CIW through various optional processes [32].
- RDF: Refuse Derived Fuel.
- WEEE: Waste Electric and Electronic Equipment.

Waste fuels are very inhomogeneous, typically enriched in high calorific value plastics, textiles, paper/cardboard, organics, wood, metals, glass, etc. Vainikka [28] reported the typical composition of MSW and SRF as shown in Table 2. Waste fuels typically contain higher amounts of halogens (F, Cl, Br) than biomass fuels, although the Cl content of some biomass fuels such as straw is high.

## 2. BACKGROUND

Table 2. Typical composition of SRF and MSW and lower heating value (LHV) in MJ/kg dry solids [33]. The composition data has been compiled from various sources [32, 34-36] and values should be taken as indicative. (Source: [28])

	SRF (wt%)	MSW (wt%)
Organics	NA <sup>a</sup>	30-40
Paper/Cardboard	40-50	15-25
Textiles	10-14	1-5
Plastics	25-35	7-15
Metals	} 2	3-4
Glass		4-7
wood	3-10	NA <sup>b</sup>
Other	5-10	18-30
<b>LHV(MJ/kg)</b>	19	11
<b>Renewable energy (%)</b>	39%	52%

NA: not analyzed

<sup>a</sup> Organic residues in SRF included in "Other"

<sup>b</sup> Wood in MSW included in "Organics"

### 2.3 Sources of halogens (F, Cl, Br) in waste fuels

#### *Chlorine*

It is generally known that chlorine (Cl) in municipal solid waste (MSW) originates mainly from chlorinated plastics, e.g., polyvinyl chloride (PVC), or food residues containing dietary salt, e.g., sodium chloride (NaCl) [8, 14]. According to Ma and Rotter [8], about 70% of the Cl in MSW originates from plastics, particularly PVC; the other sources of Cl are from kitchen waste, paper, textiles and wood. The concentration of Cl in MSW is typically ranging from 0.5-1 wt% [11, 17].

#### *Bromine*

Bromine (Br) in antropogenetic waste originates mainly from brominated flame retardants (BFRs), which are commonly found in specific waste fractions from electrical and electronic equipment (WEEE) (i.e. circuit boards, TV and PC housings), insulation foams used in the

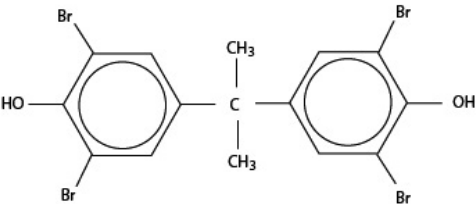
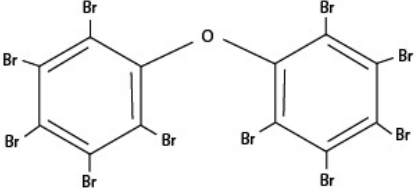
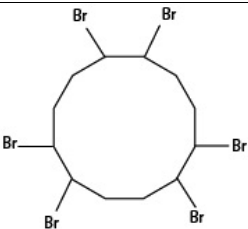
## **2. BACKGROUND**

---

building sector, and flame retarded textiles and fabrics used in upholstery and furniture cushions. The three most widely used BFRs today and over the past 10-20 years of the plastic era are tetrabromobisphenol A (TBBPA), decabromodiphenyl ether (DecaBDE) and hexabromocyclododecane (HBCD) [14]. The structural formulas of the three BFRs are shown in Table 3. It has been shown that the Br content in WEEE can be up to several wt%. A typical Br concentration in mixed MSW was indicated to be about 50-200 mg/kg; this value can increase if the waste fuels are rich in flame-retarded plastics and textiles [11, 16, 17]. In addition, bromine is widely used as both a disinfectant and a biocide in both industrial (e.g., pulp and paper mills and cooling water systems) and residential (pool, spa, and household detergents) water treatment systems. Because of these applications, bromine inevitably ends up in the industrial and municipal sewage sludge in concentrations ranging up to approximately 100 mg/kg. Bromine is also used in brominated soil fumigants and pesticides in agriculture; up to several 100 mg/kg of Br can be found as residual bromide in contaminated biological plants [16].

## 2. BACKGROUND

Table 3. Three main commercial brominated flame retardants (BFRs) [73]

	Structural formula	Chemical formula
TBBPA		$C_{15}H_{12}Br_4O_2$
DecaBDE		$C_{12}Br_{10}O$
HBCD		$C_{12}H_{18}Br_6$

### *Fluorine*

Fluorine is commonly used in fluoropolymers, a family of high-performance plastics that are chemically inert, non-wetting, very slippery, non-sticky, highly fire-resistant, high-temperature-resistant, highly weather-resistant, and regarded as non-toxic. Because of these extraordinary properties, fluoropolymers are used in a great variety of applications, e.g., in cable coating, silicon chips, wiring for laptop computers, cell phones, coated cookware, athletic and extreme-weather clothing, food-handling implements, and medical equipment. In 2004, global consumption of fluoropolymers reached 133 000 tons [18]. The increasing global trend of fluoropolymer use means that larger amounts of disposed products containing fluoropolymers will eventually end up in municipal waste combustion plants. Huber et al. [18] reported an investigation of waste produced in Norway in 2006, which indicated that paper (including coated



## 2. BACKGROUND

---

paper and cardboard), plastic, and textiles are the main waste fractions containing fluoropolymers and other fluorinated organic compounds. In addition, fluorides, e.g., sodium fluoride (NaF), are often added to drinking water supplies and dental products, such as toothpastes and mouth rinses, to prevent dental cavities [37]; these fluorides may also end up in MSW and sewage sludge. A few studies [10, 17, 38] have found several 100 mg/kg of F in MSW; however, this level could be much higher in some cases.

### 2.4 Release of ash-forming matter

In general solid fuels include three fractions: moisture, combustibles, and ash-forming matter (incombustibles). The combustible fraction, which is the organic fraction, consists mainly of carbon (C), hydrogen (H), and oxygen (O). All the other elements present in the fuel, except for (nitrogen) N, are potential ash forming elements. The main ash-forming elements are silicon (Si), aluminum (Al), iron (Fe), calcium (Ca), magnesium (Mg), manganese (Mn), sodium (Na), potassium (K), phosphorous (P), sulfur (S), and chlorine (Cl) [39]. The ash-forming matter can be present in three general forms, including water soluble salts (in the fuel moisture), organically associated ash-forming elements (in the combustibles), and included or excluded minerals (embedded in the combustibles or not). The ash-forming matter is transformed into ash during combustion [39-41]. In addition, metals in some waste fuels such as demolition wood waste, may enter the combustion system and stay in the ash. Although, most metal pieces can be separated and recycled from the wood waste, still some pieces, for example handles and nails on the wooden doors may pass the screening process.

During combustion, the ash-forming matter is released from the fuel in the process of devolatilization/pyrolysis and char burnout. Some of the ash-forming species volatilize followed by homogeneous nucleation and the subsequent coagulation to form the fine fly ash ( $< 1 \mu\text{m}$ ), while the non-volatilized species typically form larger ash particles ( $> 1 \mu\text{m}$ ) that form the coarse fly ash or remain in the bottom of the furnace as bottom ash.

## 2. BACKGROUND

---

### *Alkali metals, Cl and S*

In biomass fuels, alkali metals (mainly K), Cl and S are the main fine fly ash-forming elements. They are released into the gas phase in the combustion zone, where K will be present mainly as KCl(g) and/or KOH(g), Cl as HCl(g) and/or KCl(g), and S mainly as SO<sub>2</sub>(g). The gaseous K-species in the flame may react with fly ash particles or other gas components, e.g., SO<sub>2</sub>/SO<sub>3</sub>(g), forming K<sub>2</sub>SO<sub>4</sub>. When the flue gas is cooled as it passes through the boiler, the K-species may condense, either heterogeneously on fly ash particles or heat transfer surfaces, or homogeneously as submicron (aerosol) particles [24]. A schematic picture of the principal pathways of K, Cl and S in a biomass-fired boiler is shown in Figure 2. This picture however, could be influenced by variations in fuel composition and boiler operation.

Waste is a very inhomogeneous fuel containing significant amounts of incombustibles. The incombustible matters can be released during combustion, forming inorganic gas species and particulates. The alkali metals (Na, K), heavy metals (Zn, Pb), halogens (Cl, Br, F) and S are among the possible volatile elements in waste fuels. Frandsen [24] reported that based on the studies conducted so far, high temperature, reducing conditions and a high Cl/Me-ratio usually facilitate the release of metals (Me) such as Na, K, Zn, and Pb.

The release of these critical aforementioned volatile elements from biomass and waste combustion contribute to formation of low-melting, highly corrosive deposits on boiler tubes, causing high-temperature corrosion problems.

## 2. BACKGROUND

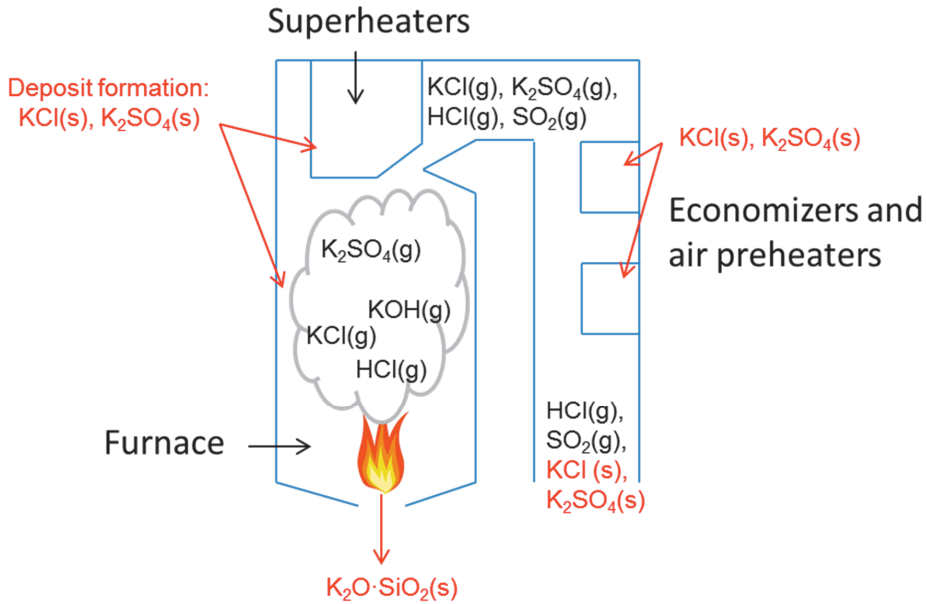


Figure 2. A schematic picture of the principal pathways of K, Cl and S in a biomass-fired boiler. (Source: revised from [4]).

### 2.5 Release of halogens

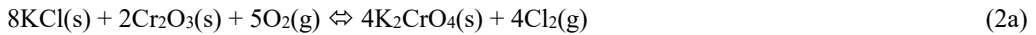
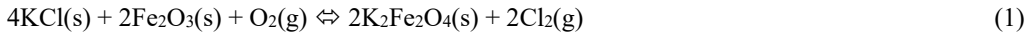
The release of halogen during biomass and waste combustion depends strongly on the chemical form of the halogen. Organic halogen compounds decompose and are released mostly as hydrogen halides (HF, HCl, HBr), with small amounts of F<sub>2</sub>, Cl<sub>2</sub> and Br<sub>2</sub> [42], or short chain halogen containing organic compounds [12]. Inorganic halogen compounds (e.g., alkali halides) may be released as HX, X<sub>2</sub> and MeX (X = F, Cl, Br; Me = Na, K). The emissions of HX from inorganic halogen compounds are generally much lower than that from organic halogen compounds (e.g., PVC), because inorganic halides do not contain easily available hydrogen [75]. Since organic halogen is the major form in WEEE, textiles and plastic waste, hydrogen halides are the major primary halogen products in waste combustion. The hydrogen halides may react with alkali metals (Na, K) released in the flue gas to form gaseous alkali halides, then condense and deposit on heat exchanger surfaces.

## 2. BACKGROUND

---

### 2.6 Alkali chloride-induced corrosion

Although the exact mechanisms behind chlorine- or alkali chloride-induced corrosion are still controversial, a common hypothesis reported in the literature is a mechanism called “active oxidation”, during which a chlorine cycle is assumed to be involved [43, 76, 77]. In “active oxidation”, chlorine is formed from a reaction between the condensed alkali chloride, e.g., KCl, and the oxide scale on the metal surface. The reaction leads also to formation of alkali ferrates and chromates (reaction 1 and reaction 2a). In the presence of water vapor, reaction 2b is supposed to take place [44]. The chlorine gas, which is formed according to reactions 1 and 2a, is speculated to penetrate the oxide layer to the scale/metal interface, where it reacts with the metal to form metal chlorides (reaction 3). Because of the high vapor pressure of the metal chlorides, vaporization will take place. The volatile metal chlorides diffuse outward through cracks and pores of the scale to the scale/gas interface, where the metal chlorides are converted into metal oxides at a higher oxygen pressure (reactions 4a and 4b). The formed oxide scale has a highly porous structure and no protection against further corrosion. The chlorine released according to reactions 4a and 4b is speculated to penetrate the damaged oxide scale and react again according to reaction 3 [43].



### 2.7 Bromine- or fluorine-induced corrosion

Literature regarding the corrosion behavior of alloys in bromine- or fluorine-containing environments, such as HBr, Br<sub>2</sub>, HF, F<sub>2</sub>, and their derivative salts of metal halides is very scarce. The possible effect of halogen on corrosion in waste incinerators was raised by Rademakers et al. [10]. They reported that alloys containing elements (e.g. Fe, Cr, Ni) which react with halogen gases (HCl, Cl<sub>2</sub>, HBr, Br<sub>2</sub>, HF, and F<sub>2</sub>) to form low-melting and/or highly volatile metal halides can suffer severe high-temperature corrosion. Research [4,45] has indicated that volatilization of a metal halide can be the dominant corrosion mechanism if the vapor pressure of the halide gas formed reaches or exceeds 10<sup>-4</sup> atm. The melting temperatures of the most important metal halides (considering the major alloying elements) and the temperatures at which their vapor pressure reaches 10<sup>-4</sup> atm are shown in Table 4. The differences in the values of comparable bromides and chlorides are minimal. Analogous to the corresponding data shown for chlorides, the temperatures at which the vapor pressures reach 10<sup>-4</sup> atm are much higher for nickel and chromium bromides than for iron bromides. Metal fluorides require much higher temperatures than metal chlorides and bromides to reach a significant vapor pressure.

## 2. BACKGROUND

Table 4. Melting points of Fe-, Cr- and Ni-chlorides, bromides, and fluorides, and the temperatures at which their vapor pressures reach  $10^{-4}$  atm [46].

Metal halides	Melting point ( °C)	Temperature at $10^{-4}$ atm ( °C)
FeCl <sub>2</sub>	676	536
FeBr <sub>2</sub>	689	509
FeF <sub>2</sub>	1020	906
FeCl <sub>3</sub>	303	167
FeBr <sub>3</sub>	-	156
FeF <sub>3</sub>	1027	673
CrCl <sub>2</sub>	820	741
CrBr <sub>2</sub>	842	716
CrF <sub>2</sub>	894	928
CrCl <sub>3</sub>	1150	611
CrBr <sub>3</sub>	> 800	615
CrF <sub>3</sub>	1404	855
NiCl <sub>2</sub>	1030	607
NiBr <sub>2</sub>	965	580
NiF <sub>2</sub>	1450	939

Vainikka et al. [15] performed a measurement campaign to determine the occurrence of corrosive ash-forming elements in a BFB boiler co-firing solid recovered fuel (SRF) with spruce bark and paper mill wastewater sludge. Alkali (K and Na) bromides and chlorides were detected in a deposit sampled from a heavily corroded area at the bottom part of the waterwalls. Iron oxide was also detected in the alkali-halide-rich area, demonstrating the contribution of halides in the corrosion process. Vainikka et al. [14] concluded that, in cases with a high level of bromine in the fuel, corrosive high-vapor pressure bromides can be formed in a manner similar to that of chlorides.

Before this work started, there was no available experimental data on the high-temperature corrosion behavior of alloys exposed to alkali bromide or fluoride salt deposits. Accordingly, the research presented in **Paper III and Paper IV** focused on lab-scale high-temperature corrosion tests of different superheater tube materials exposed to KBr or KF. The objective was to obtain a

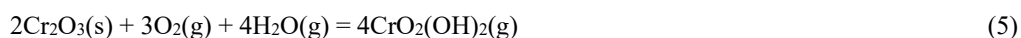
## 2. BACKGROUND

---

better understanding of the role of KBr and KF in high-temperature corrosion of superheater steels.

### 2.8 The effect of water vapor on high-temperature corrosion

Biomass and waste fuels commonly contain significant amounts of moisture. The effect of water vapor on high-temperature corrosion has not yet been satisfactorily clarified, although it is clear that it is an important parameter. Superheater tubes are often made of Fe-Cr and Fe-Cr-Ni alloys. These materials withstand high-temperature corrosion relying on the formation of a protective Cr-rich oxide scale. This protective oxide usually consists of a corundum-type solid solution  $(\text{Cr,Fe})_2\text{O}_3$ . The oxide properties depend on the chromia content and generally the higher the Cr/Fe ratio the more protective the oxide. However, it was reported that in the presence of water vapor, such protective oxide is depleted in Cr, leading to a poorly protective Fe-rich oxide, thereby reducing the expected performance life of the alloys [47]. Asteman et al. [48,49] investigated the oxidation of 304L steel in  $\text{O}_2 + 10\% / 40\% \text{H}_2\text{O}$  environments at 500-800 °C. They proposed that chromium vaporizes in the form of chromium oxide hydroxide  $(\text{CrO}_2(\text{OH})_2)$  via reaction 5, which leads to chromium depletion from the protective oxide, resulting in the formation of a poorly protective Fe-rich oxide and thus an increased oxidation rate.



Pettersson et al. [44] studied the corrosion of a 304L steel exposed to KCl in 5%  $\text{O}_2$  and in 5%  $\text{O}_2 + 40\% \text{H}_2\text{O}$  at 600 °C. The corrosion was more severe in the latter case. This observation was explained to be mainly due to the joint effect of chromium depletion by evaporation of  $\text{CrO}_2(\text{OH})_2$  via reaction 5 and the formation of  $\text{K}_2\text{CrO}_4$  via reaction 2b.

However, Lehmusto et al. [50,51] reported an opposite effect of water vapor on corrosion of 304L [51], 10CrMo and Alloy 625 [50] in the presence of KCl at 500-600 °C. It was observed that thinner oxide layers were formed under wet conditions than under dry conditions. Two explanations were suggested: (1) water causes the oxide layer to be denser and thus thinner; (2) KCl might form volatile species such as HCl in the presence of water, which would leave with

## 2. BACKGROUND

---

the surrounding gas flow and thus decrease the amount of reactive chloride in the system [50]. The first explanation is a methodological artifact of the experimental method, which only measures the thickness of the oxide layer, whereas the second explanation is connected to the reaction mechanisms. No conclusive evidence for either explanation was given. Okoro et al. [74] investigated the effect of water vapor content in the flue gas (containing HCl, SO<sub>2</sub>, CO<sub>2</sub>, O<sub>2</sub> and N<sub>2</sub>) on the corrosion of austenitic stainless steel (TP 347H FG) in the presence of KCl. They also found a decrease in the corrosion product thickness with an increase in the water vapor concentration. They suggested that a competitive adsorption on active sites of the deposit particles may influence on the corrosion process. Above a critical water vapor concentration, with the increased active site coverage by adsorbed H<sub>2</sub>O vapor, the available sites for adsorption of other species such as SO<sub>2</sub> became restricted. The authors suggested this will cause a decrease in the sulfation of KCl as well as HCl generation from the sulfation process, and hence the lower extent of corrosion.

### 2.9 Sulfation of alkali chlorides

The sulfation of alkali chlorides is important relating to aerosol formation, ash deposition and high temperature corrosion, as well as the emissions of acidic gas species, mainly HCl and SO<sub>2</sub>. Alkali halides induced high-temperature corrosion problems can be reduced either by co-combustion with sulfur rich fuels (e.g., coal, peat), or by the use of elemental sulfur or other sulfur/sulfate-containing additives such as ammonium sulfate ((NH<sub>4</sub>)<sub>2</sub>SO<sub>4</sub>) [1, 52, 53].

Glarborg [54] reported that the formation of alkali sulfates from alkali chlorides includes both homogeneous and heterogeneous mechanisms. In the heterogeneous mechanism, a gas phase alkali-containing precursor is transported to a surface where it is then sulfated by reactions in condensed or solid phases. The homogeneous mechanism involves the formation of alkali sulfate in the gas phase followed by condensation onto the deposition surfaces. The sulfation rate of KCl was found to be considerably faster in the gas phase than in the condensed phase [55].

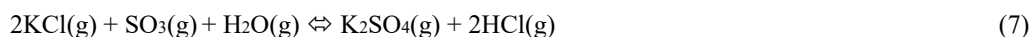
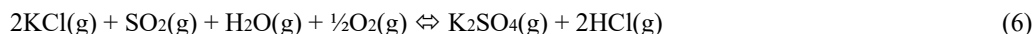
Reactions 6-9 as shown below are the most relevant reactions concerning sulfation of gaseous KCl. The sulfur required in reaction 6 can originate either from the fuel itself or from additives.



### 3. EXPERIMENTAL

---

The sulfation rate in the gas phase was found to be limited by the presence of SO<sub>3</sub>, and the oxidation of SO<sub>2</sub> to SO<sub>3</sub> (reaction 9) was claimed to be the rate-limiting step in the formation of alkali sulfate [52, 56, 57].



Glarborg and Marshall [57] suggested a more detailed and complex sulfation mechanism involving intermediate (e.g., KSO<sub>3</sub>Cl, KHSO<sub>4</sub>) steps. However, the intermediates have not been experimentally identified.

Prior to this work, there was no data available on the sulfation of alkali bromide during biomass and waste combustion, not to mention any data on the competition of sulfur in the simultaneous presence of alkali chloride and alkali bromide.

## 3. EXPERIMENTAL

The experimental work includes bench-scale BFB tests (**Papers I and II**) and laboratory-scale high temperature corrosion tests (**Papers III, IV and V**).

### 3.1 Bench-scale BFB tests

In **Papers I and II**, a series of bench-scale BFB tests were carried out. Spruce bark was used as the base fuel and served as a source of alkali metals (mainly K). HCl and HBr gases were fed with the fluidization air to simulate co-firing of a halogen-rich fuel with bark, forming and releasing alkali halides into the flue gas. SO<sub>2</sub> and elemental S powder were used as additives to study the conversion of the alkali halides to less corrosive alkali sulfates. The objectives were to

### 3. EXPERIMENTAL

---

establish a better understanding on the fate of chlorine and bromine, especially the formation of alkali halides and their sulfation behaviors in BFB combustion conditions.

#### 3.1.1 The bench-scale BFB reactor

The experiments and measurements were done in an electrically stabilized 20 kW<sub>th</sub> bubbling fluidized bed (BFB) reactor. The BFB reactor has been described earlier in several publications [58-60]. The schematic picture of the reactor is shown in Figure 3. The reactor has a bed diameter of 0.16 m. The freeboard zone has a diameter of 0.23 m and a height of 3.5 m. The interior walls that may be in contact with the flames are made of ceramics and quartz. The bed material used in the tests was natural sand with a mean particle diameter of 0.33 mm (0.1-0.6 mm) and a composition (wt%) of 3.0 Na<sub>2</sub>O, 2.3 K<sub>2</sub>O, 0.59 MgO, 2.3 CaO, 11.8 Al<sub>2</sub>O<sub>3</sub>, 1.4 Fe<sub>2</sub>O<sub>3</sub> and 77.5 SiO<sub>2</sub>. The mean gas velocity in the reactor was about 0.5 m s<sup>-1</sup>, corresponding to a total residence time of 7-8 s. This flow velocity is sufficient to transport particles up to 100 μm to the cyclone, while larger particles will deposit on the walls in the freeboard or stay in the bed. Fly ash particles of > 10 μm will be separated by the cyclone. The total residence time in the reactor is longer than in a typical BFB boiler since the upper half of the freeboard is designed to be a well-controlled zone for sampling and observation. The air staging was kept constant (primary/secondary/tertiary, 50:30:20). The bed temperature was kept between 850 and 870 °C.

### 3. EXPERIMENTAL

---

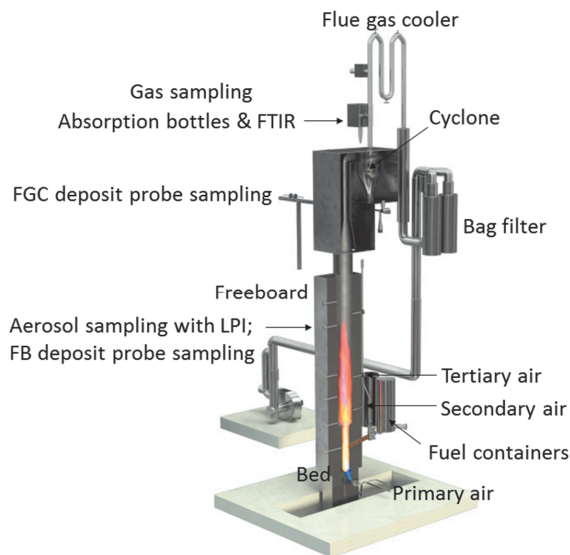


Figure 3. A schematic picture of the 20 kW<sub>th</sub> BFB reactor. FB = freeboard, FGC = flue gas channel (from Paper I and Paper II).

#### 3.1.2 Flue gas analysis

The flue gas sampling was done after the flue gas passed through a cyclone, where the flue gas temperature was between 380 and 450 °C (Figure 3). The dried flue gases (O<sub>2</sub>, CO<sub>2</sub>, CO, NO, SO<sub>2</sub>) were analyzed with standard on-line analyzers. The wet and hot (180 °C) flue gases (H<sub>2</sub>O, CO<sub>2</sub>, CO, NO, SO<sub>2</sub>, HCl) were measured by Fourier Transform Infrared Spectroscopy (FTIR). HCl, Cl<sub>2</sub>, HBr and Br<sub>2</sub> in the flue gas were sampled by absorption bottles and analyzed by ion chromatography, according to the EPA Method 26 – Determination of hydrogen halide and halogen emissions from stationary sources (non-isokinetic method) [61]. Figure 4 shows a schematic picture of the absorption bottles. Six impingers are placed in an ice water bath. The first empty bottle is called “condensation bottle”. When the cooled flue gas passes through, water will be condensed and stay in the first bottle. HBr and HCl will be partially absorbed in the first bottle, since they will dissolve in the condensed water. Br<sub>2</sub> and Cl<sub>2</sub> are not absorbed, since they are only slightly soluble in cold water. The second and the third bottle contains an acidic

### 3. EXPERIMENTAL

absorbing solution, 0.1 M sulfuric acid ( $\text{H}_2\text{SO}_4$ ), which is used to collect hydrogen halides (HBr and HCl); while the fourth and fifth bottle contains an alkaline absorbing solution, 0.1 M sodium hydroxide (NaOH), which is used to collect the halogens ( $\text{Br}_2$  and  $\text{Cl}_2$ ). The sixth bottle filled with silica gel is used to dry the flue gas. The flow rate of the flue gas passed through the six absorption bottles was 2.0 l/min. The sampling time was 1 h.

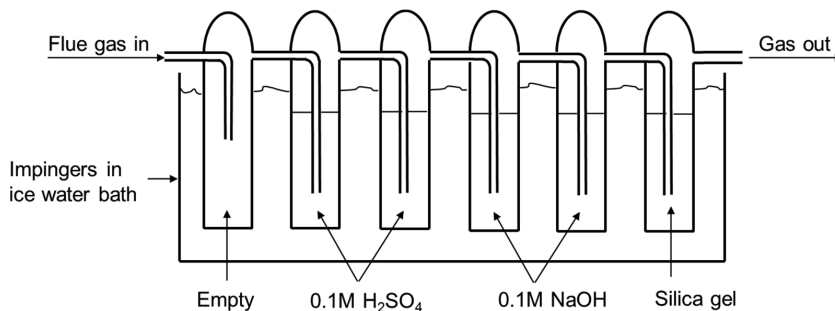


Figure 4. A schematic picture of the absorption bottles used for collection of bromine and chlorine (from Paper I).

#### 3.1.3 Aerosol sampling

“Aerosols” is a general term for a suspension of particles or droplets in gas. In this work, the term “aerosols” are defined as fine particles with an aerodynamic diameter ( $d_p$ ) less than  $1 \mu\text{m}$ , which are formed from vaporized ash-forming elements prevailing at fluidized bed combustion temperatures. These vapors nucleate and/or condense to form fine particles in a cooling flue gas or in an aerosol sampling probe. In biomass and waste firing, the vaporized halogen-containing salts are assumed to be the main carriers of halogen to the superheater surfaces, thereby leading to halogen-induced corrosion. The aerosols in the flue gas were sampled by a Decati<sup>®</sup> low pressure impactor (DLPI) in the upper part of the freeboard (Figure 3), where the flue gas temperature was about  $870 \text{ }^\circ\text{C}$ .

The aerosol sampling was carried out by means of a combination of an air-cooled gas permeable tube probe and two consecutive ejector dilutors. A schematic diagram of the aerosol sampling arrangement is shown in Figure 5. The sample gas was sucked into the probe and immediately

### 3. EXPERIMENTAL

diluted with nitrogen and quenched within a 200 mm long gas permeable tube diluter. The targeted dilution ratio (DR) of this first dilution stage was 4. The sample gas was taken from the probe to a second dilution stage, where it was diluted by an ejector diluter with DR = 8. After the dilutions the sample gas was divided between two parallel Dekati<sup>®</sup> low pressure impactors (DLPI) and one electric low pressure impactor (ELPI). At the location of the division a third gas stream was taken to an FTIR gas analyzer for determination of the exact total dilution ratio on the basis of H<sub>2</sub>O and CO<sub>2</sub>. The reference H<sub>2</sub>O and CO<sub>2</sub> concentrations for determination of the total dilution ratio were measured with the FTIR at the location after the cyclone as shown in Figure 3. Before the actual aerosol sampling (DLPI and ELPI), each gas line was equipped with a pre-cutter cyclone to remove particles larger than 10 μm. Furthermore, a third dilution stage was used with a DR = 11 before the ELPI. With the ELPI, the number-size distribution of particles can be observed on-line.

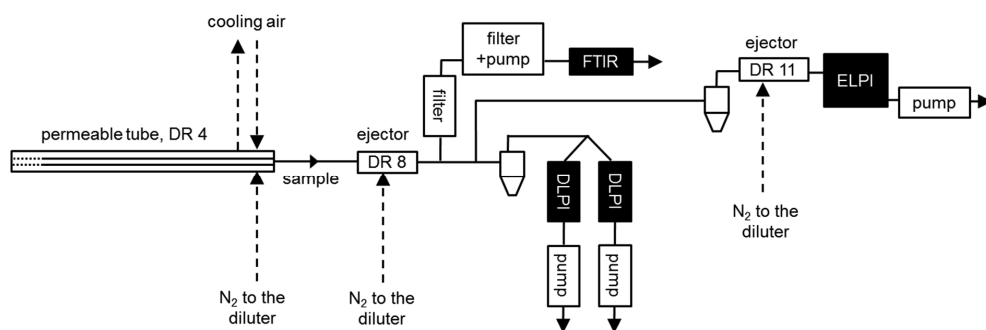


Figure 5. A schematic picture of the aerosol sampling installation. Revised from [62].

DLPI is a cascade low pressure impactor, which has 13-stages so that airborne particles are size classified into 13 size fractions. The particle size is in the range of 0.03-10 μm. A schematic picture of DLPI is shown in Figure 6. When the flue gas passes through the impaction nozzle of each impactor stage (following the blue streamlines), it is turned sharply before the collection substrate. Particles larger than the stage cut-off diameter cannot follow the flow streamlines and will impact on the collection substrate. While particles smaller than the stage cut-off diameter will continue to the next impactor stage where they are further size classified and collected. By

### 3. EXPERIMENTAL

changing the dimensions in each impactor stage, different sized particles can be collected on different impactor stages [63]. Table 5 shows the cut-off diameter  $D_{50}$  of each stage.  $D_{50}$  means the particle diameter for 50% of collection efficiency, in other words, 50% of the particles bigger than this diameter will be collected on the substrate and 50% of them will pass [64]. The particle size distribution in DLPI is determined by gravimetric and chemical analysis of the collected particles [63]. The results can be in the form of mass concentration. The composition of particles collected on each stage was determined by a scanning electron microscope equipped with an energy-dispersive X-ray detector (SEM/EDX).

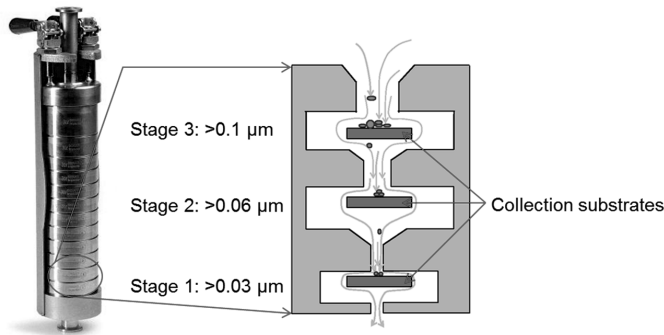


Figure 6. A schematic picture of the Dekati<sup>®</sup> low pressure impactor (from Paper I).

Table 5. The cut diameter  $D_{50}$  of each impactor stage (from Paper I).

Stage	1	2	3	4	5	6	7	8	9	10	11	12	13
$D_{50}$ , [ $\mu\text{m}$ ]	0.03	0.06	0.09	0.16	0.26	0.39	0.62	0.96	1.61	2.41	4.02	6.73	9.99

#### 3.1.4 Deposit sampling

Two air-cooled deposit probes were used in the tests. As shown in Figure 3, one probe was placed in the upper part of the freeboard (FB), where the gas temperature was about 870 °C; the other probe was placed in the flue gas channel (FGC) before the cyclone, where the flue gas temperature was about 600 °C. The surface temperature of both probes was kept at 500 °C. The deposit sampling time was 3 h. After the tests, deposits from the windward, 90° side, and leeward positions were taken and analyzed by SEM/EDX.

### 3. EXPERIMENTAL

#### 3.2 Laboratory-scale high-temperature corrosion tests

In **Papers III, IV and V**, a series of laboratory-scale high-temperature corrosion tests were carried out. Three different superheater steel materials were used in the experiments: a low-alloy steel (10CrMo9-10), an austenitic stainless steel (AISI 347), and a high chromium and nickel austenitic stainless steel (Sanicro 28). Table 6 presents the elemental compositions of the steels. The dimensions of the steel samples were  $20 \times 20 \times 5$  mm (length  $\times$  width  $\times$  thickness). Before the corrosion test, the steel samples were polished in ethanol using 600 and 1000 grit SiC papers, washed in an ultrasound bath, and then pre-oxidized for 24 h at 200 °C. After the pre-treatment, the steel samples were covered with 0.25 g of KBr, KF or KCl with a particle size of 30-100  $\mu$ m, placed in a horizontal tube furnace, and heat-treated at different temperatures (400-600 °C) in ambient air (also called “dry air” in **Paper III** and **Paper IV**), wet air (containing 30 vol% H<sub>2</sub>O), or other three gas atmospheres (2% H<sub>2</sub>O-30% O<sub>2</sub>-N<sub>2</sub>, 2% H<sub>2</sub>O-2% O<sub>2</sub>-N<sub>2</sub> and 30% H<sub>2</sub>O-2% O<sub>2</sub>-N<sub>2</sub>) for 168 h (7 days). After the heat treatment, the samples were removed from the furnace, cooled to room temperature, and cast directly in a polyester resin. Each sample was then cut off in the middle to reveal the cross-section. The cross-section surfaces of the samples were then polished in kerosene using 1000 and 1200 grit SiC papers and cleaned with petroleum ether in an ultrasound bath. The samples were then carbon-coated and analyzed by SEM/EDX.

Table 6. The elemental compositions of the tested steels (wt%) as analyzed with SEM/EDX.

	Fe	Cr	Ni	Mo	Mn	Si	C	Nb	P	S
10CrMo9-10	95.96	2.24	-	1.00	0.45	0.25	0.07	-	0.01	0.01
AISI 347	68.74	18.08	10.92	-	0.92	0.46	0.04	0.81	0.02	0.01
Sanicro 28 (S28)	36.11	27.36	31.38	3.51	1.15	0.46	0.01	-	0.01	0.01

The oxide layer thickness and the thickness distribution were measured at some 10 000 points over a 4 mm representative region of the cross-section using a panorama SEM technique, which has been described in detail in earlier publications [65-68]. The corrosion attack was expressed as the mean thickness of the oxide layer. The elemental distributions in the oxide layer, steel and salt were identified by EDX.

## 4. RESULTS AND DISCUSSION

### 4.1 BFB test results

#### 4.1.1 Formation of alkali halides (Paper I)

Particles in the range of 0.03-10  $\mu\text{m}$  were collected by the DLPI. In this work, the discussion is focused on the major elements Na, K, Cl, Br, Ca and S, since, according to the SEM/EDX analyses, these elements covered almost 100 wt% of the fine particles ( $< 1 \mu\text{m}$ ), and  $\sim 70$  wt% of the coarse particles (1–10  $\mu\text{m}$ ). The rest  $\sim 30$  wt% of the coarse particles consisted of Mg, Al, Si, P, Mn, Fe and Zn, which represented the mineral composition of the original fuel (spruce bark). The concentrations of these elements were generally not influenced by the addition of HBr and/or HCl.

The mass concentrations and compositions of the collected particles in the different aerodynamic particle sizes ( $\mu\text{m}$ ) for the “Bark”, “Bark+HBr”, “Bark+HCl” and “Bark+HBr+HCl” cases are shown in Figure 7. The mass size distribution of the particles in each test was found to be bimodal. In the “Bark” case, where only bark was burned, the particle size distribution showed a lower peak at around 0.16  $\mu\text{m}$  for fine particles and a higher peak at around 4.02  $\mu\text{m}$  for coarse particles. During addition of HBr and/or HCl (Tests “Bark+HBr”, “Bark+HCl” and “Bark+HBr+HCl”), the peak for fine particles became higher, but at a lower particle size, around 0.06  $\mu\text{m}$ . The addition of HBr and/or HCl in different proportions strongly increased the formation of fine particles, compared to the “Bark” case.

In the “Bark” case, it can be seen that the fine particles consisted mainly of K, S, and Cl. According to Christensen and Livbjerg [69], the initiation of the fine particle formation is the homogeneous nucleation of vapor species that are derived from non-combustible material in the fuel. Consequently, all the K, Cl, and S in the fine particles have been in gaseous form after combustion. With addition of HBr and/or HCl (Tests “Bark+HBr”, “Bark+HCl” and “Bark+HBr+HCl”), only alkali halides, almost no sulfates, were found in the fine particles. Furthermore, it was clear that the addition of HBr or HCl greatly increased the release of alkali



#### 4. RESULTS AND DISCUSSION

metals (K, Na) from the original fuel (spruce bark) during combustion. The promoting effect of HBr (Test “Bark+HBr”) was more obvious than that of HCl (Test “Bark+HCl”). This also indirectly indicated that HBr was more reactive towards the alkali metals than HCl.

In the “Bark+HBr+HCl” case, with equal amounts of HCl and HBr, the concentration of the fine particles showed a clear difference between the Cl and Br compounds, a higher amount of Br than of Cl bonded to alkali metals. These results were also supported by the deposit (Figure 8) and flue gas (Figure 9) analyses.

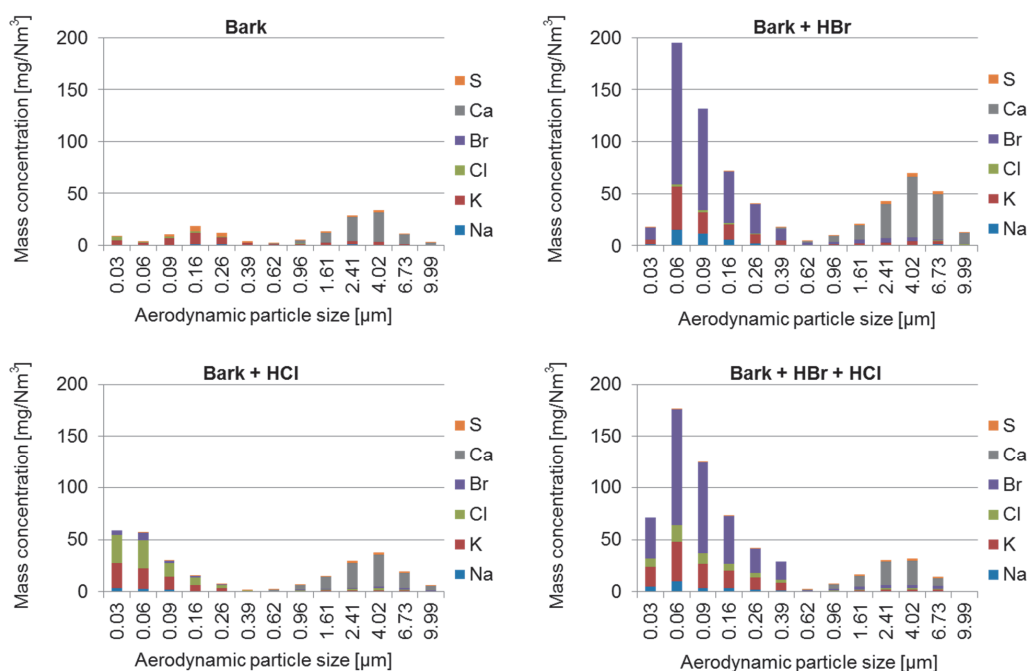


Figure 7. The mass size distributions and elemental (S, Ca, Br, Cl, K, Na) concentrations of the particles collected by the DLPI in the “Bark”, “Bark+HBr”, “Bark+HCl” and “Bark+HBr+HCl” cases (revised from Paper I).

Figure 8 shows the elemental compositions (S, Ca, Br, Cl, K, Na) of the ash deposit at different ring locations in the “Bark+HBr+HCl” case. The deposit composition was clearly dependent on the location on the ring (windward, 90° side and leeward). The alkali metals (K, Na) and

#### 4. RESULTS AND DISCUSSION

halogens (Cl, Br) were mostly concentrated in the deposit at the 90° side; also higher amount of Br than Cl was found to be bonded to alkali metals.

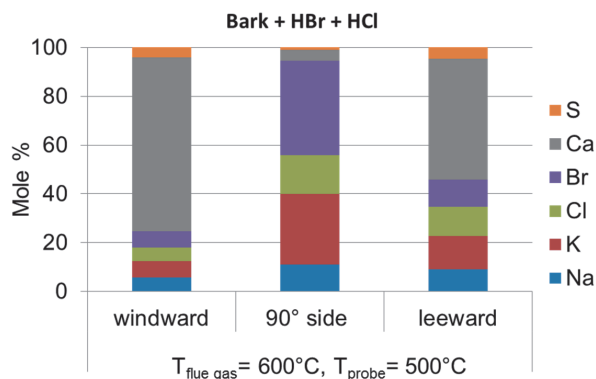


Figure 8. The elemental compositions (S, Ca, Br, Cl, K, Na) of the ash deposit at different ring locations in the “Bark+HBr+HCl” case (revised from Paper I).

Figure 9 shows the concentrations of HCl and HBr in the flue gas in the “Bark”, “Bark+HBr”, “Bark+HCl” and “Bark+HBr+HCl” cases. The red-lined bar in the “Bark+HCl” case means that the HBr should not exist there, but was anyway detected because of some memory effect from the previous test. In the “Bark+HBr+HCl” case, equal amounts of HCl and HBr was fed, but less HBr than HCl was found to be left in the flue gas. This indirectly indicates a higher tendency for HBr than HCl to form alkali halides.

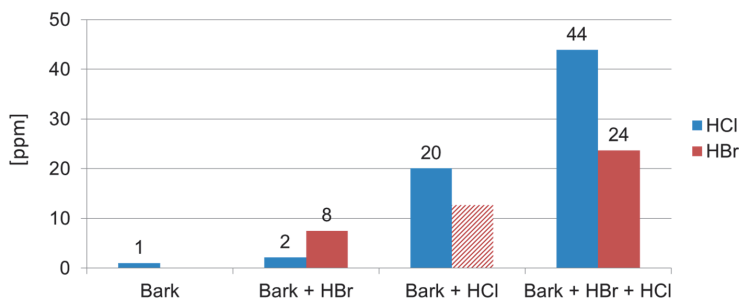


Figure 9. The concentrations of HCl and HBr in the flue gas in the “Bark”, “Bark+HBr”, “Bark+HCl” and “Bark+HBr+HCl” cases.

## 4. RESULTS AND DISCUSSION

### 4.1.2 Sulfation of alkali halides (Paper II)

In **Paper II**, the sulfation behavior of alkali chloride and alkali bromide was studied. Figure 10 shows the concentrations of the major elements in the fine particles ( $< 1 \mu\text{m}$ ) in the cases with and without S addition.

In these four cases, the molar ratios of Br:Cl:S were 12:12:1 (Ref), 12:12:25 (Bark+HBr+HCl+Low S), 0:24:25 (Bark+HCl+Low S), and 24:0:25 (Bark+HBr+Low S). The total molar amount of the sum of both added halogens was kept the same in all cases, and the amount of added S was the same in the latter three cases.

Comparing the first two cases, after S addition, the concentration of Br in the fine particles decreased from  $4.1 \text{ mmol/Nm}^3$  in the reference case to  $2.1 \text{ mmol/Nm}^3$  in the “Bark+HBr+HCl+Low S” case, while for the concentration of Cl, from  $1.4 \text{ mmol/Nm}^3$  to  $0.5 \text{ mmol/Nm}^3$ . This indicates that a higher share of alkali chlorides than bromides was sulfated. Furthermore, by comparing the latter two cases between each other, a lower amount of Cl ( $1.2 \text{ mmol/Nm}^3$ ) than Br ( $2.9 \text{ mmol/Nm}^3$ ) was found in the fine particles. This also indicates a higher sulfation extent of alkali chlorides than alkali bromides.

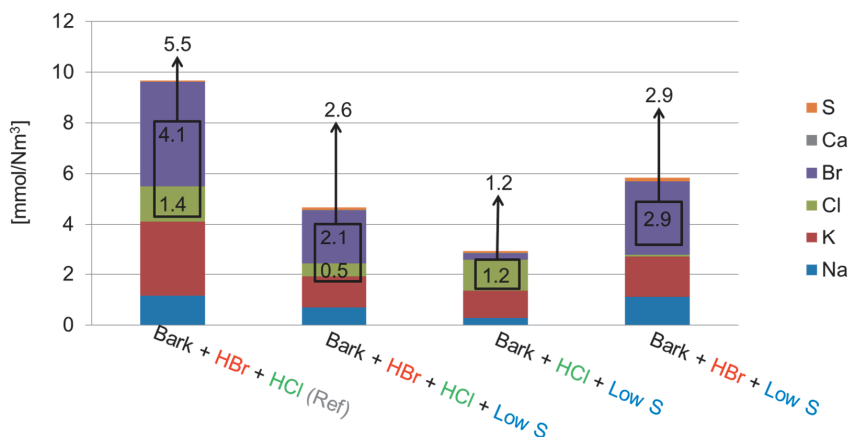


Figure 10. The concentrations of the major elements in the fine particles ( $< 1 \mu\text{m}$ ) (revised from Paper II).

## 4. RESULTS AND DISCUSSION

---

In addition, the thermodynamic calculations presented in **Paper II** indicated that the sulfation of KCl is thermodynamically more favorable than KBr, which well supported the experimental results.

### 4.2 Laboratory corrosion test results

#### 4.2.1 Potassium halide-induced corrosion in dry conditions (Paper III)

The mean oxide layer thickness values of all cases with KBr or KF in ambient air (also called “dry air” or “dry conditions” in the thesis and in **Paper III** and **Paper IV**) are summarized in Figure 11 and Table 7. The results were also compared to tests with KCl from Enestam et al. [70]. At relatively low temperatures ( $\leq 550$  °C), all tested salts (KBr, KF and KCl) were equally corrosive. At 600 °C, KF showed much stronger corrosivity than KBr and KCl, especially for 10CrMo9-10 and AISI 347.

The corrosion attack was generally more severe at higher temperatures. 10CrMo9-10 suffered from the highest degree of corrosion. The alloying elements, Cr and Ni, in the austenitic steels (AISI 347 and Sanicro 28), clearly increased their corrosion resistance. The higher content of Cr and Ni in Sanicro 28 than in AISI 347 did not necessarily improve the performance of Sanicro 28; in fact, Sanicro 28, in some cases, performed even worse than AISI 347, as strongly localized corrosion attacks were observed.

#### 4. RESULTS AND DISCUSSION

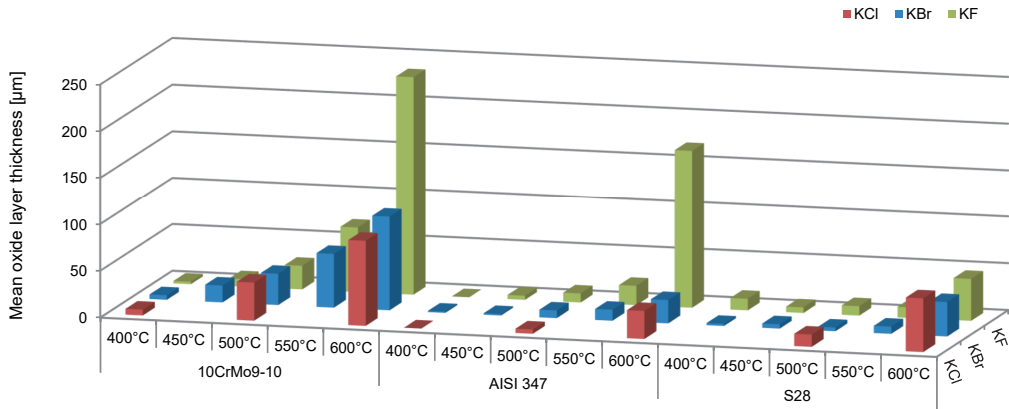


Figure 11. Mean oxide layer thicknesses of the three steels, 10CrMo9-10, AISI 347 and Sanicro 28 (S28), exposed to KBr, KF and KCl for 168 h in ambient air at different temperatures. KCl data taken from Enestam et al. [70] (from Paper III).

Table 7. Detailed mean oxide layer thicknesses [µm]. The “-” sign indicates no test.

	10CrMo9-10					AISI 347					S28				
	400 °C	450 °C	500 °C	550 °C	600 °C	400 °C	450 °C	500 °C	550 °C	600 °C	400 °C	450 °C	500 °C	550 °C	600 °C
KCl	6	-	41	-	91	0	-	5	-	30	-	-	13	-	57
KBr	5	18	33	57	100	1	2	8	12	25	2	5	4	8	37
KF	3	8	25	69	233	0	4	10	21	168	12	6	10	11	45

Figure 12 shows the SEM and X-ray maps of 10CrMo9-10 exposed to KBr and KF at 600 °C in ambient air. 10CrMo9-10 suffered from extreme corrosion with both KBr and KF. In the case with KF, K was observed in the oxide layer in the same regions as Fe and O, indicating the presence of a K-Fe-oxide, probably potassium ferrate ( $K_2Fe_2O_4$ ). However, this K-Fe-oxide was not observed in the case with KBr. Most likely the formation of potassium ferrate significantly destroyed the protectiveness of the oxide layer, thereby leading to 10CrMo9-10 suffering from much higher corrosion with KF than with KBr.

#### 4. RESULTS AND DISCUSSION

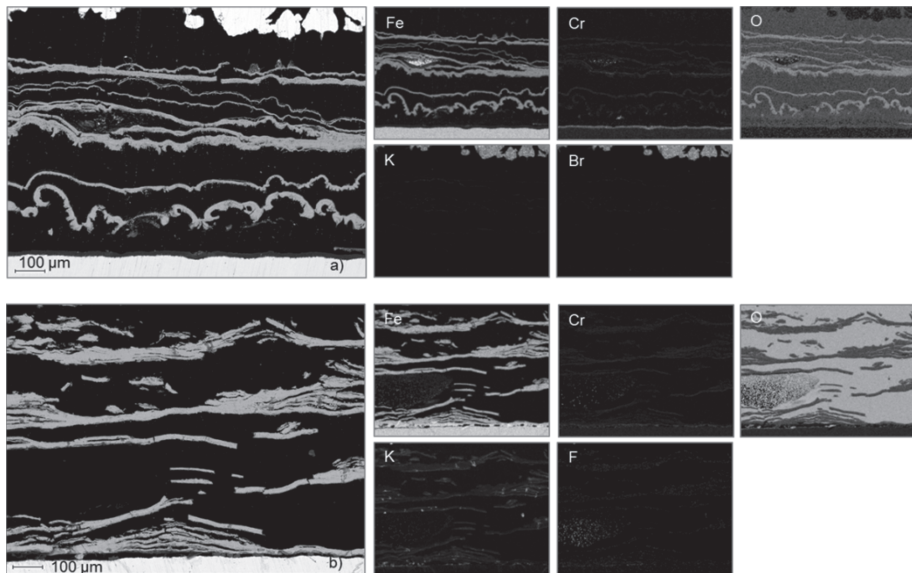


Figure 12. SEM and X-ray images of 10CrMo9-10 exposed to (a) KBr and (b) KF at 600 °C in ambient air for 168 h (revised from Paper III).

Figure 13 shows the SEM and X-ray maps of AISI 347 exposed to KBr and KF at 600 °C in ambient air. In the case of AISI 347 with KBr (Figure 13a), the inner oxide layer close to the steel consisted of a Fe-Cr-Ni oxide, below which a nickel-rich metallic layer remained on the steel surface due to the depletion of Fe and Cr; the outer oxide layer consisted of K, Cr and O, most likely  $K_2CrO_4$  (potassium chromate) based on the quantification analysis. This  $K_2CrO_4$  was formed locally on top of the Fe-Cr-Ni oxide. Furthermore, this  $K_2CrO_4$  appears to have been partially molten together with KBr at 600 °C. This may be related to the findings of a study by Shinata [71], who reported the role of  $Na_2CrO_4$  in accelerated oxidation of Cr induced by NaCl. Shinata proposed that  $Na_2CrO_4$  decreased the melting point of NaCl by forming a NaCl- $Na_2CrO_4$  eutectic with a reported temperature of 577 °C. Once the eutectic mixture was formed, the oxidation reaction continued in the melt or through the melt, which prevented the formation of a protective scale. The same mechanism can be speculated to be valid for the test with KBr, in which a KBr- $K_2CrO_4$  eutectic was most likely formed and played a similar role in the accelerated

#### 4. RESULTS AND DISCUSSION

oxidation. The eutectic temperature was reported to be 629 °C [72], which is close to the test temperature.

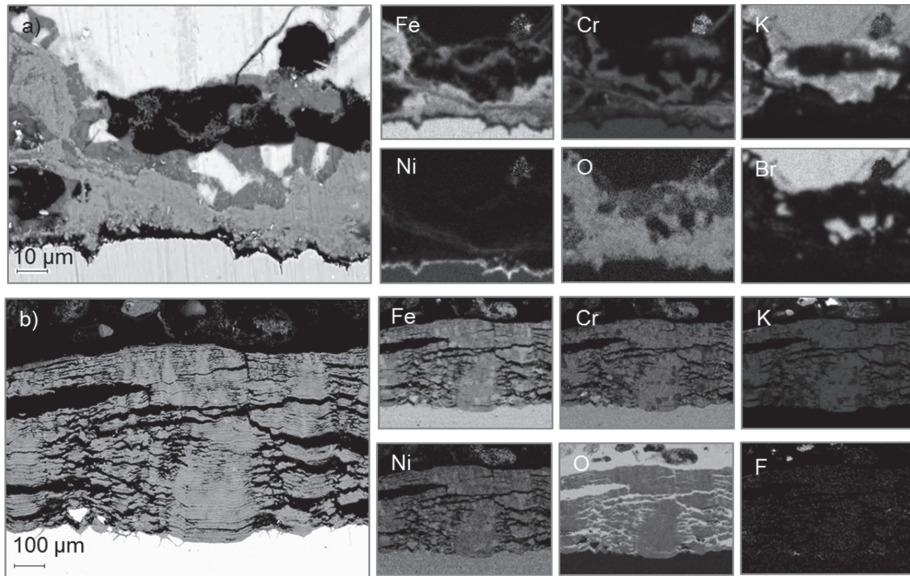


Figure 13. SEM and X-ray images of AISI 347 exposed to (a) KBr and (b) KF at 600 °C in ambient air for 168 h (revised from Paper III).

In the case of AISI 347 with KF (Figure 13b), no melt was observed between the oxide scale and the salt particles. A Fe-Cr-Ni oxide together with K but not with F was observed on AISI 347. K was most likely in the form of  $K_2CrO_4$ , assuming that KF performed in a manner similar to KCl and KBr, initiating the “active oxidation” by destroying the protective  $Cr_2O_3$ . Furthermore, the fact that no F was observed in the oxide scale implies that it exited in gaseous form.

In addition, much more metal (Fe, Cr, and Ni) oxidation occurred in the test with KF (Figure 13b) than with KBr (Figure 13a) at 600 °C. Also, Ni was found throughout the oxide layer in the test with KF, which is different as it was observed in the test with KBr, with a Ni-rich metallic layer remained on the steel surface due to the depletion of Fe and Cr. However, it cannot simply be explained by the volatilization and outward diffusion of metal halide, followed by oxidation at the scale/gas interface, because the vapor pressures would indicate that the metal (Fe, Cr, and Ni)

#### 4. RESULTS AND DISCUSSION

bromides are more volatile than the corresponding metal fluorides (Table 3). As shown in Figure 13b, a large amount of K (assumed as  $K_2CrO_4$ ) is embedded throughout the oxide layer in the test with KF, while in the case with KBr,  $K_2CrO_4$  was formed locally just on top of the Fe-Cr-Ni compact oxide (Figure 13a). In the case with KF, the significant formation of  $K_2CrO_4$  probably increased the porosity of the oxide layer and assisted the inward diffusion of  $O_2$ , which can enhance the inward oxidation of metal fluorides close to the scale/metal interface. This may explain why significant metal (Fe, Cr, and Ni) oxidation occurred without the volatilization of metal fluorides at 600 °C.

Figure 14 shows the SEM and X-ray maps of Sanicro 28 exposed to KBr and KF at 600 °C in ambient air. The oxide layer structure of Sanicro 28 with KBr and KF looks very similar to that of AISI 347 with KBr and KF. In the case of Sanicro 28 exposed to KF (Figure 14b), a continuous F-rich layer was observed at the metal/scale interface and along the grain boundaries. This F was most likely in the form of KF and (Fe, Cr, Ni)-fluorides.

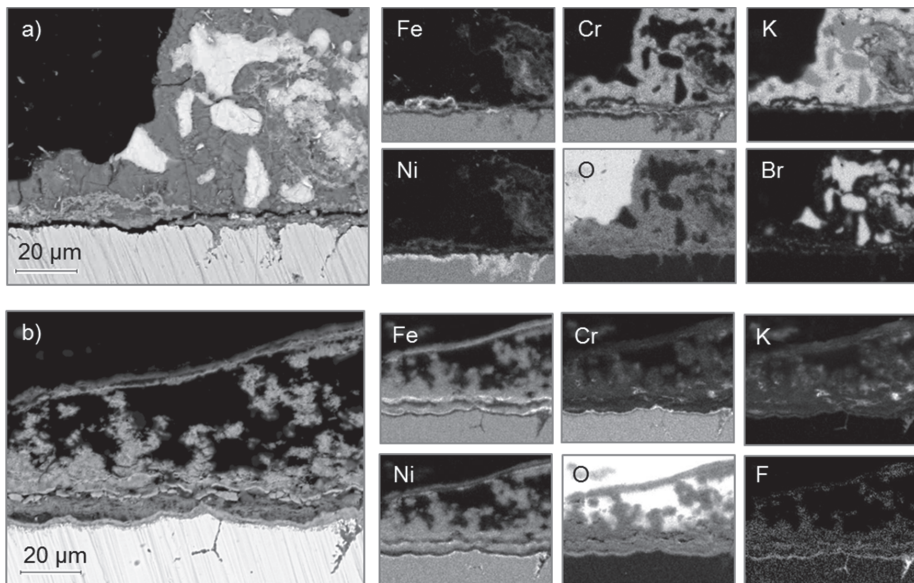


Figure 14. SEM and X-ray images of Sanicro 28 exposed to (a) KBr and (b) KF at 600 °C in ambient air for 168 h. (revised from Paper III).



##### 4.2.2 Potassium halide-induced corrosion in wet conditions (Paper IV)

Figure 15 shows the mean oxide layer thickness values for tests done in ambient air (also called “dry air” or “dry conditions” in the thesis and in **Paper III** and **Paper IV**) and wet air (30% H<sub>2</sub>O) at 450 and 550 °C. The results marked with the symbol “x” represent duplicate samples showing the reproducibility of the tests.

The corrosion layers developed on all three tested steels were generally thicker at the higher test temperature (550 °C) in both ambient air and wet air. At 450 °C, the effect of water vapor was not obvious. At 550 °C, the influence of water vapor became significant in some cases, but the trend was not consistent. For instance, in the case of 10CrMo9-10 with KBr, the oxide layer was much thicker in wet air than in ambient air, while with KCl and KF, the oxide layers were thinner in wet air.

In the case of Sanicro 28 with KCl at 550 °C, a very thick oxide layer (113 µm) was formed in ambient air, while in wet air the formed oxide layer was just 2 µm thick. On the other hand, when Sanicro 28 was exposed to KF at 550 °C in wet air an increased oxide layer growth was observed. The results for AISI 347 with all the three salts were similar in both ambient air and wet air.

In ambient air at 550 °C, the corrosivity of the three test salts was in most cases similar for each specific test steel. The sole exception was KCl which resulted in an extreme corrosion of Sanicro 28.

Among the 10CrMo9-10 cases in wet air at 550 °C, KBr showed much higher corrosivity than KCl and KF. In the cases of the two austenitic steels (AISI 347 and Sanicro 28) in wet air at 550 °C, KF appeared to be more corrosive than KCl and KBr.

In general, the corrosion resistance of AISI 347 was shown to be the best among the three tested steels at 450 and 550 °C.

#### 4. RESULTS AND DISCUSSION

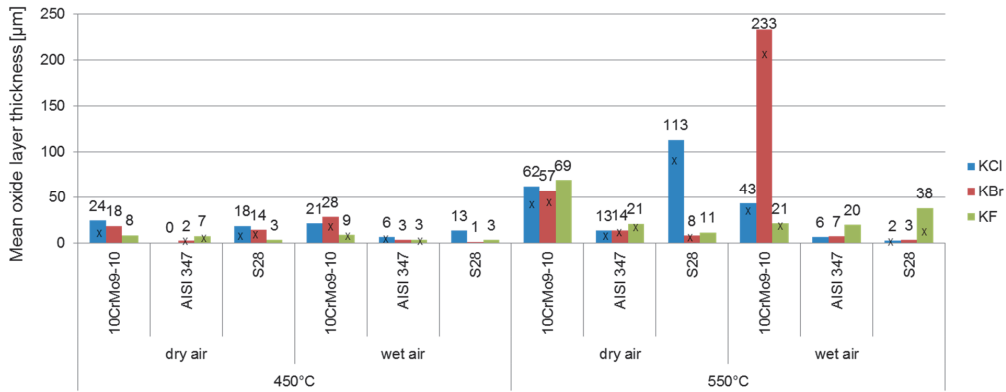


Figure 15. Mean oxide layer thicknesses of the three steels, 10CrMo9-10, AISI 347 and Sanicro 28 (S28), exposed to KCl, KBr, and KF for 168 h in ambient air (also called “dry air” or “dry conditions” in the thesis and in **Paper III** and **Paper IV**) and wet air (30% H<sub>2</sub>O) at 450 °C and 550 °C (from Paper IV).

#### 4.2.3 Comparison the corrosion behavior in dry and wet conditions (**Papers III and IV**)

In this chapter, the corrosion behavior of each steel (10CrMo9-10, AISI 347 and Sanicro 28) exposed to KCl, KBr and KF in ambient air (also called “dry air” or “dry conditions” in the thesis and in **Paper III** and **Paper IV**) and wet air (30% H<sub>2</sub>O) is discussed.

##### 10CrMo9-10

##### 10CrMo9-10 exposed to KBr

Figure 16 shows panorama SEM images of 10CrMo9-10 exposed to KBr at 550 °C in ambient air and wet air (30% H<sub>2</sub>O) for 168 h. 10CrMo9-10 suffered from much higher corrosion in wet air than in ambient air. On top of a dense oxide layer, a more significant development of porous iron oxide growing around salt particles was observed in wet air (Figure 16b).

#### 4. RESULTS AND DISCUSSION

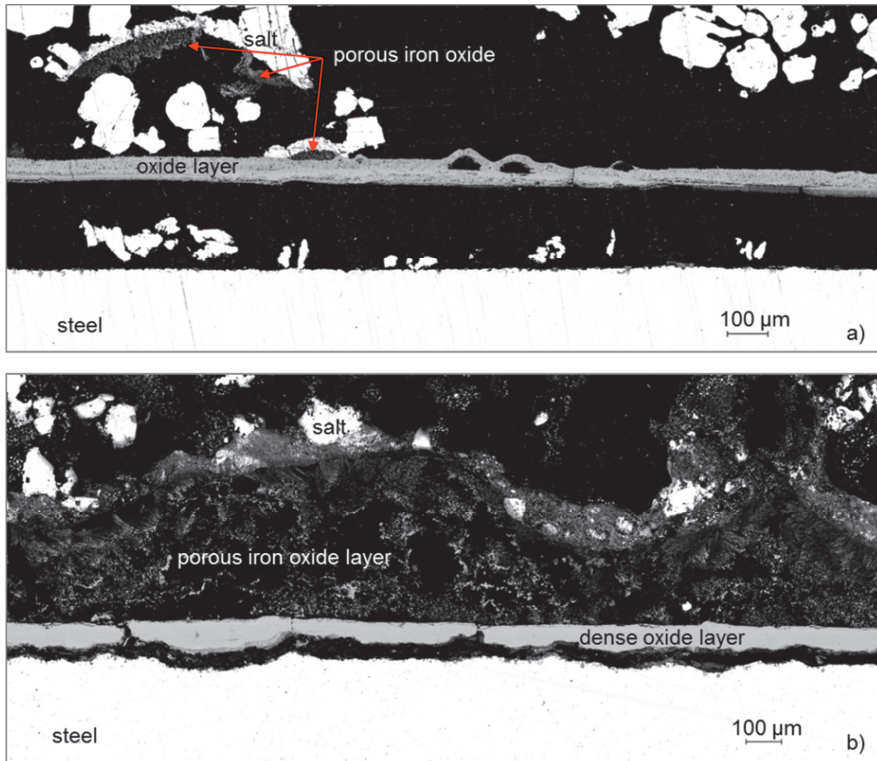


Figure 16. Panorama SEM images of 10CrMo9-10 exposed to KBr at 550 °C in (a) ambient air and (b) wet air (30% H<sub>2</sub>O) for 168 h (from Paper IV).

#### 10CrMo9-10 exposed to KF and KCl

In the case of 10CrMo9-10 exposed to KF (Figure 17) and KCl (Figure 18) at 550 °C, the influence of water vapor was the opposite of that observed in the case of 10CrMo9-10 exposed to KBr (Figure 16).

#### 4. RESULTS AND DISCUSSION

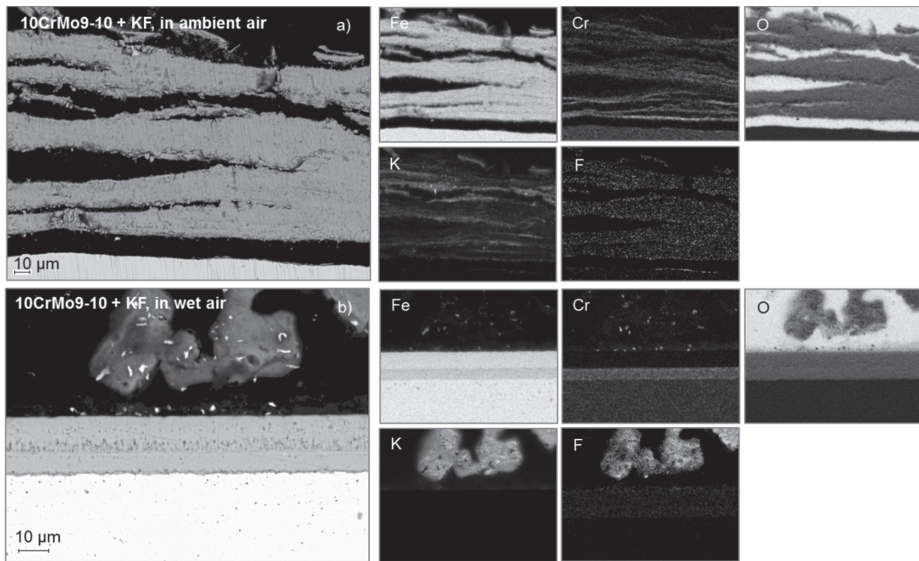


Figure 17. SEM and X-ray images of 10CrMo9-10 exposed to KF at 550 °C in (a) ambient air and (b) wet air (30% H<sub>2</sub>O) for 168 h (from Paper IV).

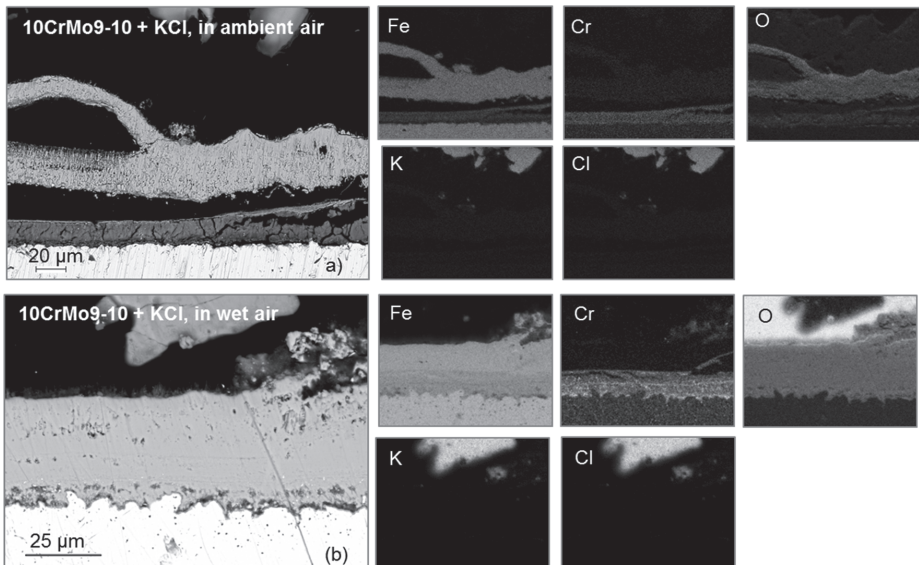


Figure 18. SEM and X-ray images of 10CrMo9-10 exposed to KCl at 550 °C in (a) ambient air and (b) wet air (30% H<sub>2</sub>O) for 168 h (revised from Paper IV).

#### 4. RESULTS AND DISCUSSION

---

In the case of 10CrMo9-10 exposed to KF in ambient air at 550 °C (Figure 17a), a very thick and uneven oxide layer was formed. The scale had a multi-layered structure and consisted mainly of Fe-oxide and a small amount of Cr-oxide. Furthermore, K was distributed in the oxide layer in the same regions as Fe and O, indicating the presence of a K-Fe-oxide, probably potassium ferrate ( $K_2Fe_2O_4$ ). However, this kind of K-Fe-oxide was not observed in the cases of 10CrMo9-10 exposed to KCl and KBr in either ambient or wet air.

In the case of 10CrMo9-10 exposed to KF in wet air (30% H<sub>2</sub>O) at 550 °C, a much thinner, well-adherent and even oxide layer was formed (Figure 17b). K was not observed in the oxide layer here as it had been observed in the ambient air case.

Figure 18 shows the SEM and X-ray maps of 10CrMo9-10 exposed to KCl at 550 °C in ambient and wet air (30% H<sub>2</sub>O) for 168 h. The elemental distributions in the oxide layer in both cases are very similar. Fe was distributed throughout the oxide layer, with some enrichment in the outer part, while Cr was present only in the inner oxide layer just above the steel surface.

Compared to the oxide layer formed in the ambient air case (Figure 18a), the oxide layer formed in the wet air case (Figure 18b) was thinner, more compact, more even, and better adhered to the steel surface. This observation is similar to the aforementioned results in the case of 10CrMo9-10 exposed to KF (Figure 17). However, K was not observed in the cases of 10CrMo9-10 exposed to KCl in either ambient air or wet air. In addition, internal oxidation along the grain boundaries was observed on 10CrMo9-10 exposed to KCl in wet air (Figure 18b).

#### **AISI 347**

##### AISI 347 exposed to KBr and KCl

At 550 °C, AISI 347 showed similar corrosion behavior under KCl and KBr in both ambient air and wet air (30% H<sub>2</sub>O). The differences in the corrosion behaviors did not result from the salt but rather from the gas atmosphere. Therefore, the cases of AISI 347 exposed to KBr are shown as an example in the following discussion.

#### 4. RESULTS AND DISCUSSION

Figure 19 shows the SEM and X-ray images of AISI 347 exposed to KBr at 550 °C in ambient air and wet air for 168 h. Potassium chromate was formed and distributed in the Fe-Cr-Ni oxide layer in ambient air (Figure 19a) but not in wet air (Figure 19b). The scale formed on AISI 347 under KBr in wet air (Figure 19b) had a better adherence to the steel surface and had a more compact structure than the scale formed in ambient air (Figure 19a). In addition, internal oxidation occurred in wet air. The internal oxide layer consisted of Fe-, Cr-, and Ni-oxides, whereas the outer scale contained only Fe-oxide. The protectiveness of the original chromia film is lost, probably due to the formation of volatile chromium oxide hydroxide ( $\text{CrO}_2(\text{OH})_2$ ) via reaction 5 [48]. Therefore, only the non-protective external scale of Fe-oxide is left, beneath which at the scale/metal interface the oxygen partial pressure is sufficiently high for the metal to be internally oxidized.

In ambient air it seems that the salt (KBr or KCl) is the trigger to the destruction of the protectiveness of  $\text{Cr}_2\text{O}_3$  by formation of  $\text{K}_2\text{CrO}_4$ , whereas in wet air, the water vapor may be the trigger via the formation of volatile  $\text{CrO}_2(\text{OH})_2$ , since no K-chromates were detected.

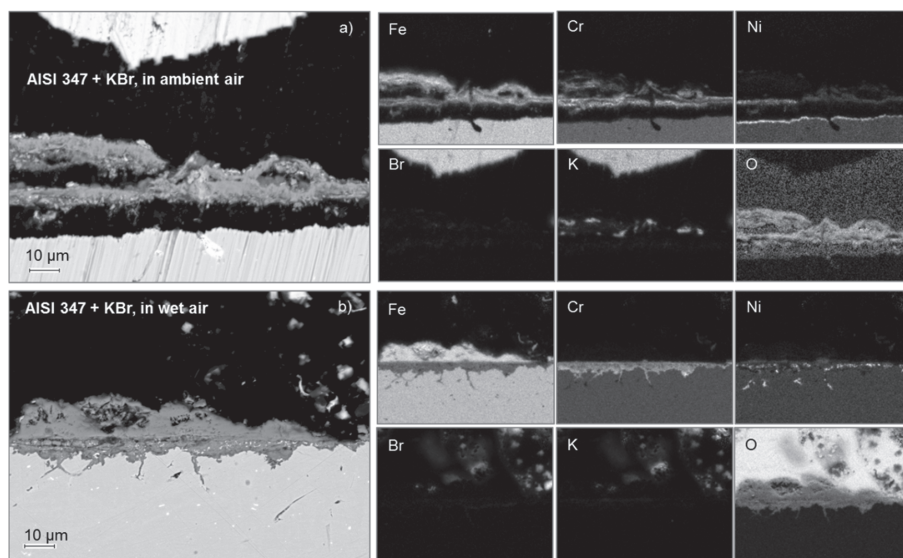


Figure 19. SEM and X-ray images of AISI 347 exposed to KBr at 550 °C in (a) ambient air and (b) wet air (30%  $\text{H}_2\text{O}$ ) for 168 h (from Paper IV).

#### 4. RESULTS AND DISCUSSION

##### AISI 347 exposed to KF

Figure 20 shows the SEM and X-ray images of AISI 347 exposed to KF at 550 °C in ambient air and wet air (30% H<sub>2</sub>O) for 168 h. In both cases, the whole oxide layer consisted of Fe, Cr, Ni, together with K but no F was found. K was most likely in the form of K<sub>2</sub>CrO<sub>4</sub>. In the ambient air case, some F (most likely as KF) was also detected in the oxide layer (Figure 20a), while in the wet air case (Figure 20b), no F was detected in the whole oxide layer. The signal of F observed in the X-ray map was probably from O.

In the ambient air case, the oxide layer was very even, while in the wet air case, local deep pitting corrosion occurred. The deepest pitting was about 50 μm in depth. Such deep pitting corrosion can cause serious local damage to the steel. For such a case with an uneven oxide layer, the average thickness value does not correctly reflect the real corrosion behavior. Therefore, it is important to consider this kind of corrosion separately.

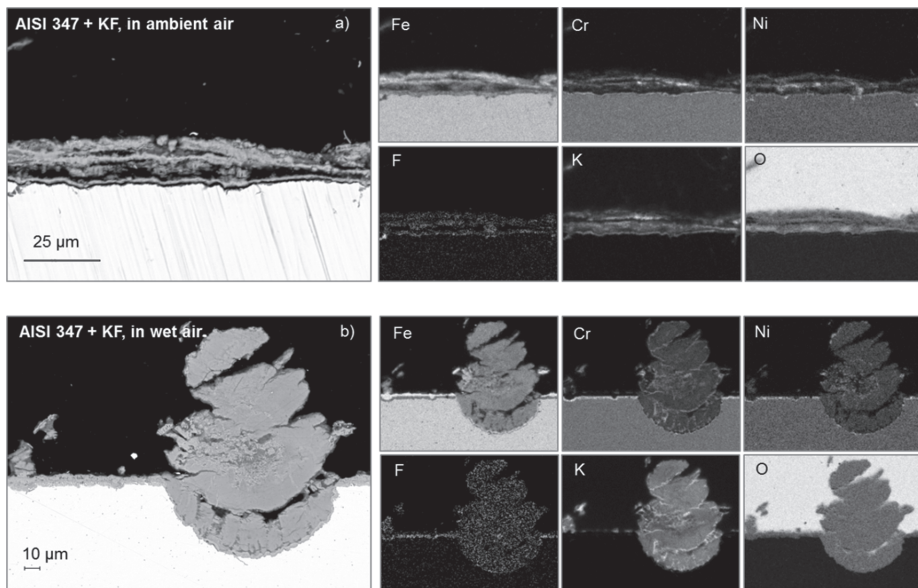


Figure 20. SEM and X-ray images of AISI 347 exposed to KF at 550 °C in (a) ambient air and (b) wet air (30% H<sub>2</sub>O) for 168 h (revised from Paper IV).

#### 4. RESULTS AND DISCUSSION

### Sanicro 28

#### Sanicro 28 exposed to KBr and KCl

Figure 21 and Figure 22 show the SEM and X-ray maps of Sanicro 28 exposed to KBr and KCl at 550 °C in ambient air and wet air (30% H<sub>2</sub>O) for 168 h. It can be seen that Sanicro 28 exposed to KBr (Figure 21b) or KCl (Figure 22b) showed very good corrosion resistance in the wet air case, with a very thin (2-3 μm) and even oxide layer formed. However, in the ambient air case, higher corrosion occurred on Sanicro 28 exposed to KBr (Figure 21a) or KCl (Figure 22a). Especially when Sanicro 28 exposed to KCl (Figure 22a), the corrosion was extreme, with an oxide layer thickness of 113 μm. Some formation of potassium chromate was observed in both cases with KBr (Figure 21a) and KCl (Figure 22a) in ambient air.

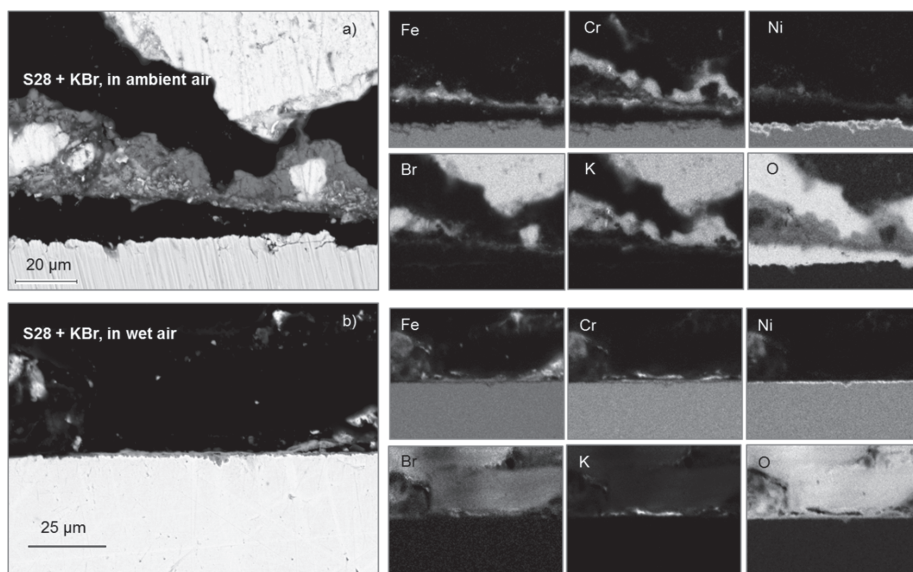


Figure 21. SEM and X-ray images of Sanicro 28 exposed to KBr at 550 °C in (a) ambient air and (b) wet air (30% H<sub>2</sub>O) for 168 h (revised from Paper IV).



#### 4. RESULTS AND DISCUSSION

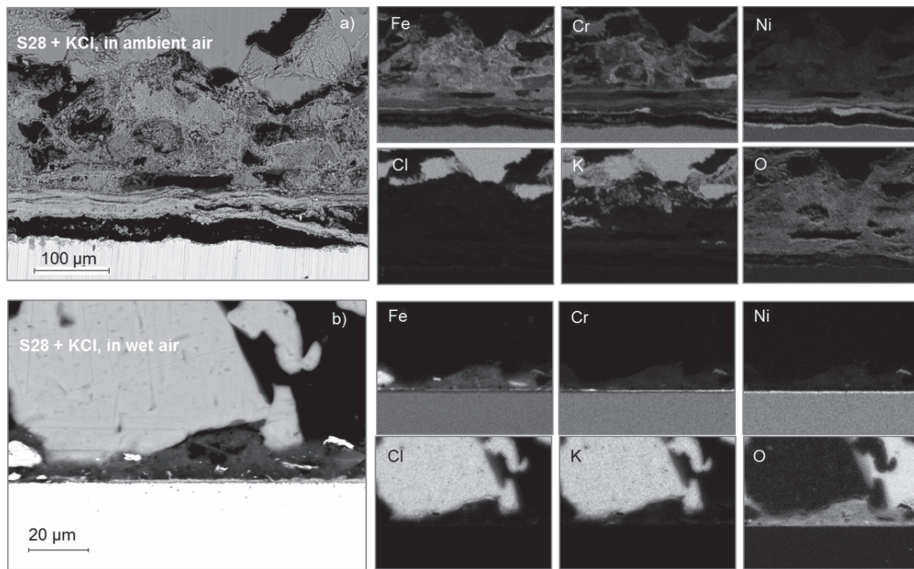


Figure 22. SEM and X-ray images of Sanicro 28 exposed to KCl at 550 °C in (a) ambient air and (b) wet air (30% H<sub>2</sub>O) for 168 h (revised from Paper IV).

Figure 22a shows that Fe and Cr were enriched in the uppermost layer of the porous oxide scale, which grew around the salt particles, indicating vaporization of iron and chromium chlorides, followed by subsequent oxidation and condensation [70]. K, but no Cl, was also present in the uppermost layer in the same region as Cr and O, suggesting the formation of potassium chromate. This confirms the reaction between KCl and Cr<sub>2</sub>O<sub>3</sub>, leading to the destruction of the protective chromia scale and allowing subsequent accelerated oxidation. The inner oxide layer consisted of Fe-, Cr- and Ni-oxides. Duplicate tests of Sanicro28 under KCl in ambient air showed a similar severe corrosion attack. The Cr and Ni content in Sanicro 28 is the highest among the three test steels, but its corrosion resistance was significantly deteriorated when exposed to KCl in ambient air.

#### 4. RESULTS AND DISCUSSION

##### Sanicro 28 exposed to KF

Figure 23 shows the SEM and X-ray images of Sanicro 28 exposed to KF at 550 °C in ambient air and wet air for 168 h. The oxide layer structure and the elemental distribution in the oxide layer are quite similar to those observed in the previous cases with AISI 347 exposed to KF in ambient air and wet air (Figure 20). In addition, as shown in Figure 24, after exposure to KF in wet air, Sanicro 28 suffered more local pitting corrosion than AISI 347. The deepest pitting depth for Sanicro 28 was about 40  $\mu\text{m}$ .

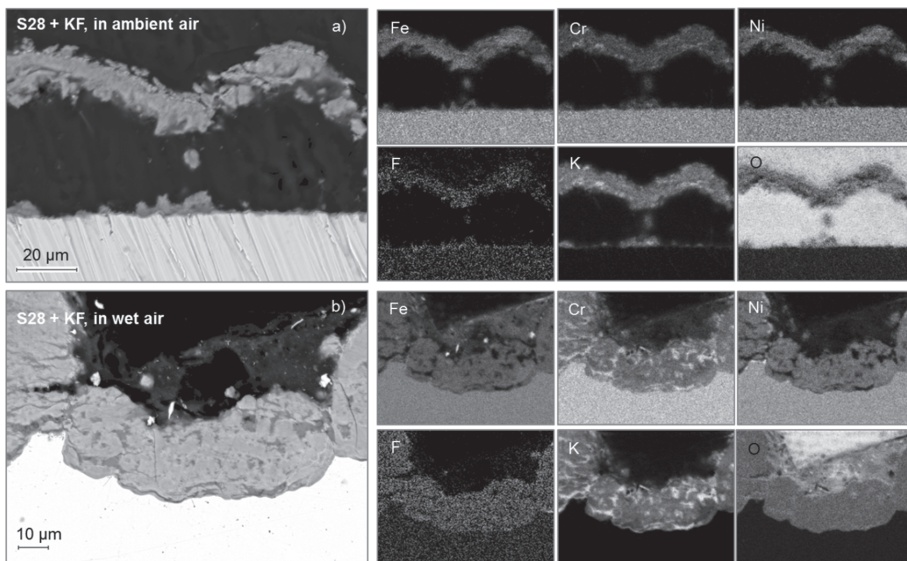


Figure 23. SEM and X-ray images of Sanicro 28 exposed to KF at 550 °C in (a) ambient air and (b) wet air (30%  $\text{H}_2\text{O}$ ) for 168 h (revised from Paper IV).

#### 4. RESULTS AND DISCUSSION

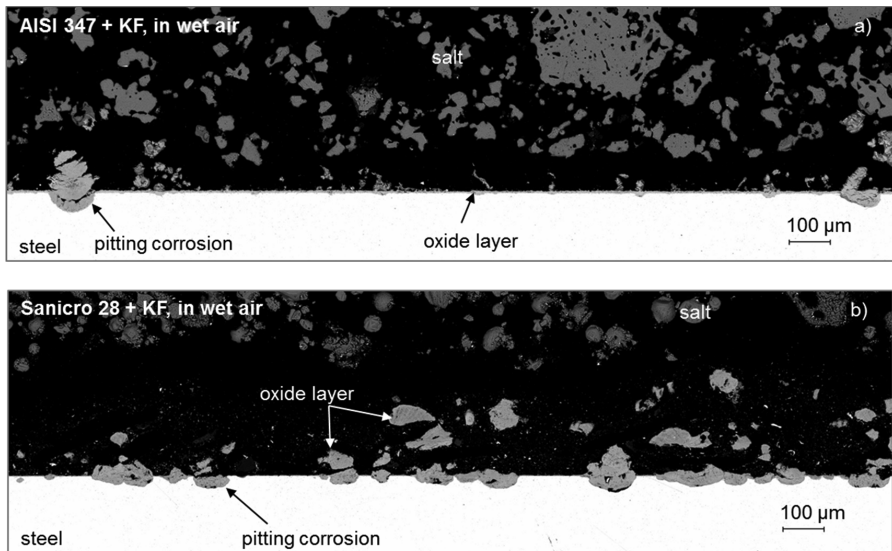


Figure 24. Panorama SEM images of (a) AISI 347 and (b) Sanicro 28 exposed to KF at 550 °C in wet air (30% H<sub>2</sub>O) for 168 h (revised from Paper IV).

#### 4.2.4 The influence of H<sub>2</sub>O/O<sub>2</sub> ratios on KCl-induced corrosion (Paper V)

In **Paper V**, the influence of H<sub>2</sub>O/O<sub>2</sub> ratios on corrosion of the three steels exposed to high temperature with and without KCl was studied. Three different gas atmospheres were used in the tests: 2% H<sub>2</sub>O-30% O<sub>2</sub>-N<sub>2</sub> (“O<sub>2</sub>-rich” atmosphere), 2% H<sub>2</sub>O-2% O<sub>2</sub>-N<sub>2</sub> and 30% H<sub>2</sub>O-2% O<sub>2</sub>-N<sub>2</sub> (“H<sub>2</sub>O-rich” atmosphere); the corresponding H<sub>2</sub>O/O<sub>2</sub> ratios were 0.07, 1 and 15, respectively. Figure 25 summarizes the results of the tests.

#### 4. RESULTS AND DISCUSSION

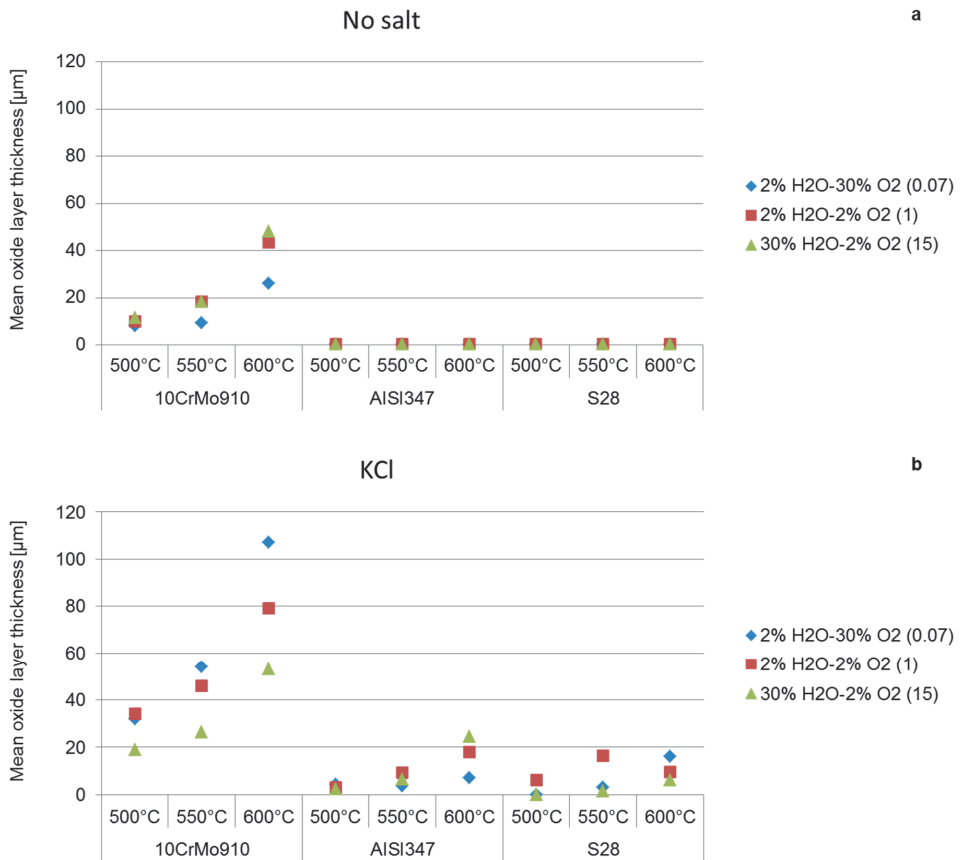


Figure 25. Mean oxide layer thicknesses of three steels, 10CrMo9-10, AISI 347 and Sanicro 28 (S28), exposed to (a) no salt and (b) KCl at 500, 550 and 600 °C in atmospheres with different H<sub>2</sub>O/O<sub>2</sub> ratios (0.07, 1, 15) (revised from Paper V).

In the tests with no salt (Figure 25a), no corrosion occurred on AISI 347 and Sanicro 28 at the test temperatures in the three different gas atmospheres; only 10CrMo9-10 showed increased corrosion with increasing temperature. At 500 °C, almost equally thin oxide layers (~10  $\mu\text{m}$ ) were formed on 10CrMo9-10 at all three gas atmospheres, showing no influence on corrosion by changing the H<sub>2</sub>O/O<sub>2</sub> ratios. At 550 and 600 °C, the lowest corrosion (~10  $\mu\text{m}$  at 550 °C and ~25  $\mu\text{m}$  at 600 °C) for 10CrMo9-10 occurred in the “O<sub>2</sub>-rich” atmosphere with a H<sub>2</sub>O/O<sub>2</sub> ratio of

#### 4. RESULTS AND DISCUSSION

---

0.07, while in the other two atmospheres, the oxide layer thicknesses were quite similar ( $\sim 20 \mu\text{m}$  at  $550 \text{ }^\circ\text{C}$  and  $\sim 45 \mu\text{m}$  at  $600 \text{ }^\circ\text{C}$ ).

Compared to the tests with no salt (Figure 25a), the oxide layers developed on the three steels were thicker in all tests with KCl (Figure 25b). Generally, all the three steels covered with KCl showed an increasing corrosion trend with increasing temperature in each gas atmosphere, although for Sanicro 28 the trend was not fully consistent. For 10CrMo9-10 with KCl, the lowest corrosion occurred in the “H<sub>2</sub>O-rich” atmosphere with a H<sub>2</sub>O/O<sub>2</sub> ratio of 15, while the highest corrosion occurred in the “high O<sub>2</sub>” atmosphere with a H<sub>2</sub>O/O<sub>2</sub> ratio of 0.07. For AISI 347 and Sanicro 28 with KCl, the influence of different H<sub>2</sub>O/O<sub>2</sub> ratios on corrosion showed no consistent trend. Low corrosion occurred on these two steels, with oxide layer thicknesses mostly less than  $20 \mu\text{m}$ . AISI 347 and Sanicro 28 showed better corrosion resistance than 10CrMo9-10 in all three gas atmospheres.

Figure 26 shows the influence of the H<sub>2</sub>O/O<sub>2</sub> ratio on corrosion of 10CrMo9-10 at 500, 550 and 600 °C. An opposite trend was clearly observed in the “no salt” and “KCl” cases, especially for the cases at 600 °C. Among the three gas atmospheres, the “O<sub>2</sub>-rich” atmosphere with a H<sub>2</sub>O/O<sub>2</sub> ratio of 0.07 was the least corrosive in “no salt” cases, but the most corrosive in “KCl” cases. In the “O<sub>2</sub>-rich” atmosphere, the presence of KCl significantly increased the corrosion. Furthermore, the increasing corrosion by the presence of KCl also increased with increasing temperature. However, in the “H<sub>2</sub>O-rich” atmosphere with a H<sub>2</sub>O/O<sub>2</sub> ratio of 15, the presence of KCl did not result in any significant differences at all the three test temperatures.

#### 4. RESULTS AND DISCUSSION

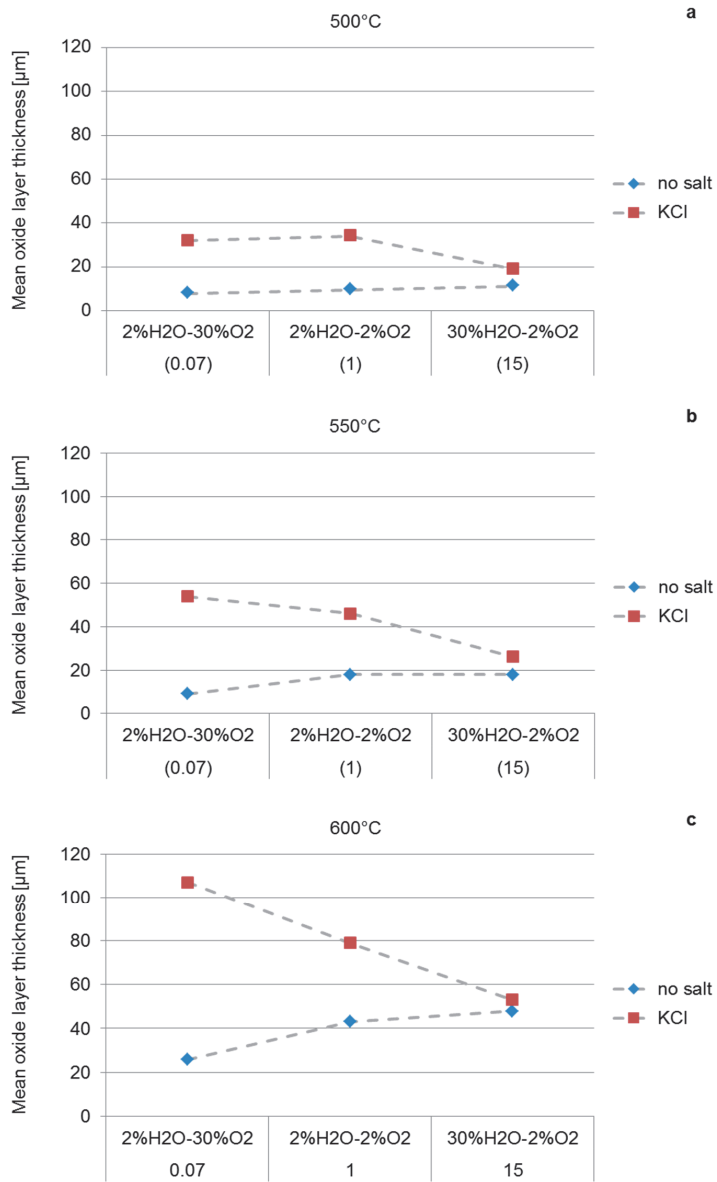


Figure 26. Mean oxide layer thicknesses of 10CrMo9-10 exposed to no salt and KCl in atmospheres with different  $\text{H}_2\text{O}/\text{O}_2$  ratios (0.07, 1, 15) at a) 500  $^{\circ}\text{C}$ , b) 550  $^{\circ}\text{C}$ , c) 600  $^{\circ}\text{C}$  for 168 h (from Paper V).

#### 4. RESULTS AND DISCUSSION

Figure 27 shows the SEM and X-ray maps of 10CrMo9-10 exposed to 600 °C both with and without KCl in the “H<sub>2</sub>O-rich” atmosphere with a H<sub>2</sub>O/O<sub>2</sub> ratio of 15 and the “O<sub>2</sub>-rich” atmosphere with a H<sub>2</sub>O/O<sub>2</sub> ratio of 0.07. As described above, the oxide layer thickness developed on 10CrMo9-10 in “H<sub>2</sub>O-rich” atmosphere was almost equal for both the “no salt” and “KCl” cases (Figures 27a and 27b). It can be observed that the morphology of the oxide scales in both cases is very even and well-adherent to the steel surface. Also, no traces of K or Cl were found in the scale (Figure 27b).

In the “O<sub>2</sub>-rich” atmosphere, the oxide layer was much thicker in the “KCl” case (Figure 27d) than in the “no salt” case (Figure 27c). Some formation of K<sub>2</sub>CrO<sub>4</sub> was observed in the case with KCl (Figure 27d).

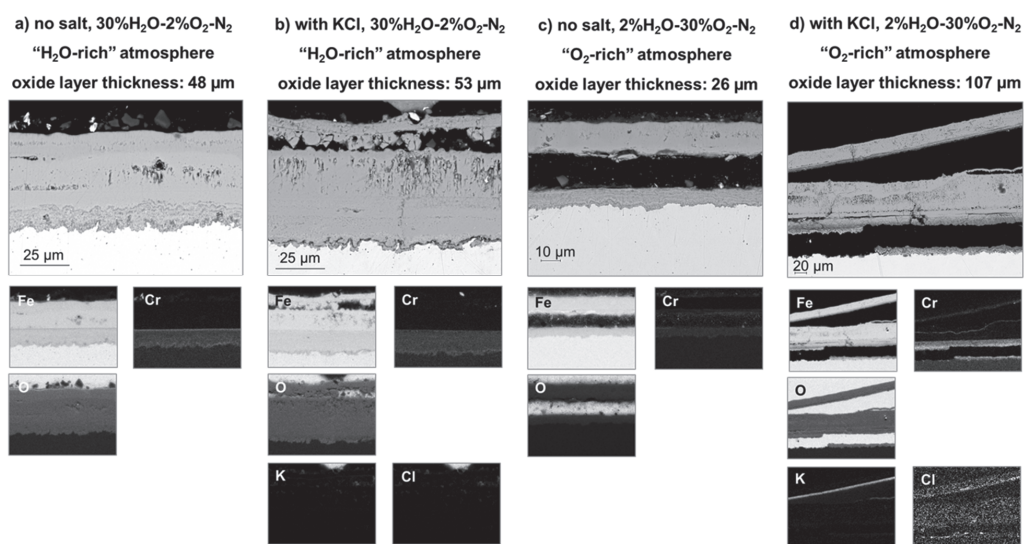


Figure 27. SEM and X-ray images of 10CrMo9-10 exposed to a) no salt and 30% H<sub>2</sub>O-2% O<sub>2</sub>-N<sub>2</sub>, b) KCl and 30% H<sub>2</sub>O-2% O<sub>2</sub>-N<sub>2</sub>, c) no salt and 2% H<sub>2</sub>O-30% O<sub>2</sub>-N<sub>2</sub>, d) KCl and 2% H<sub>2</sub>O-30% O<sub>2</sub>-N<sub>2</sub>, at 600 °C for 168 h (from Paper V).

### 5. CONCLUSIONS

In this work, a series of bench-scale BFB tests were carried out to characterize the formation and sulfation behaviors of KCl and KBr. Spruce bark was used as the base fuel - serving as a source of alkali metals (mainly K, some Na). HCl and HBr gases were fed with the fluidization air to simulate co-firing of a halide-rich fuel with bark, thereby forming alkali halide aerosols in the flue gas.

It was found that the addition of HBr or HCl greatly increased the release of alkali metals (K, Na) from the original fuel during combustion. The promoting effect of HBr was more obvious than that of HCl. Further, HBr was found to have a clearly higher tendency to form alkali halides than HCl.

In the bench-scale BFB tests, SO<sub>2</sub> and elemental S powder were used as additives to convert the alkali halide aerosols to less corrosive alkali sulfates. The sulfation extent with S was somewhat lower than with SO<sub>2</sub>, but generally on the same level. The results indicated a higher tendency for sulfation of alkali chloride than of alkali bromide. These results were also supported by thermodynamic calculations.

A series of laboratory tests were carried out to investigate the high-temperature corrosion behaviors of three different superheater steels (10CrMo9-10, AISI 347 and Sanicro 28) exposed to potassium halides in ambient air and wet air containing 30% H<sub>2</sub>O. The influence of H<sub>2</sub>O and O<sub>2</sub> on the high temperature corrosion of steels with and without KCl in three gas atmospheres (2% H<sub>2</sub>O-30% O<sub>2</sub>-N<sub>2</sub>, 2% H<sub>2</sub>O-2% O<sub>2</sub>-N<sub>2</sub> and 30% H<sub>2</sub>O-2% O<sub>2</sub>-N<sub>2</sub>) was also studied. The most important results are summarized below:

Ambient air:

At relatively low temperatures ( $\leq 550$  °C), the corrosivity of KBr and KF are similar to KCl. At 600 °C, KF showed much stronger corrosivity than KBr and KCl. When exposed to KBr or KF,



## 5. CONCLUSIONS

---

10CrMo9-10 could be durable up to 450 °C; AISI 347 and Sanicro 28 could be durable up to 550 °C.

Wet air (containing 30% H<sub>2</sub>O):

At 450 °C, the influence of water vapor was not obvious. At 550 °C, the influence of water vapor became significant in some cases, but the trend was not consistent. At 550 °C, 10CrMo9-10 suffered from much more corrosion (oxide layer thickness of 233 μm) when exposed to KBr than when exposed to KF and KCl. At 550 °C, local deep pitting corrosion occurred on AISI 347 and Sanicro 28 when exposed to KF. The deepest pitting depth was about 40-50 μm. Some formation of K<sub>2</sub>CrO<sub>4</sub> was observed in the oxide layer. At 550 °C, low corrosion was observed on AISI 347 and Sanicro 28 when exposed to KBr and KCl.

Gas atmospheres with different H<sub>2</sub>O/O<sub>2</sub> ratios:

The corrosion of 10CrMo9-10 without salt increased with increasing H<sub>2</sub>O (decreasing O<sub>2</sub>), while the corrosion of 10CrMo9-10 with KCl decreased with increasing H<sub>2</sub>O (decreasing O<sub>2</sub>). In the “O<sub>2</sub>-rich” atmosphere, the presence of KCl significantly increased the corrosion of 10CrMo9-10. However, in the “H<sub>2</sub>O-rich” atmosphere, the presence of KCl did not result in any significant differences on the corrosion of 10CrMo9-10. It is suggested that in the “H<sub>2</sub>O-rich” atmosphere, volatile CrO<sub>2</sub>(OH)<sub>2</sub> is mainly formed, while in the “O<sub>2</sub>-rich” atmosphere and in the presence of KCl, K<sub>2</sub>CrO<sub>4</sub> is mainly formed.

In the tests with no salt at 500-600 °C, no corrosion occurred on AISI 347 and Sanicro 28. In the tests with KCl at 500-600 °C, low corrosion occurred on these two steels with oxide layer thicknesses mostly under 20 μm. The influence of different H<sub>2</sub>O/O<sub>2</sub> ratios on the corrosion of these two steels showed no consistent trend.

Considering both the results from the BFB tests and the laboratory corrosion tests, if waste fuels with equal amounts of Br or Cl were to be combusted, the corrosion damage of superheaters would be expected to be higher in the bromine case. The possible formation of potassium fluoride in BFB combustion conditions has not yet been studied, which needs to be investigated in the

## ***5. CONCLUSIONS***

---

future work. Also, more detailed investigations on the effect of H<sub>2</sub>O on high-temperature corrosion needs attention, especially in the presence of possible ash compounds. Furthermore, also other salts, such as lead- and zinc bromides and/or fluorides may become important in the future due to the increasing use of demolition wood as a fuel for power and heat production.

## REFERENCES

---

## REFERENCES

- [1] Broström M., Kassman H., Helgesson A., Berg M., Andersson C., Backman R., Nordin A. *Sulfation of corrosive alkali chlorides by ammonium sulfate in a biomass fired CFB boiler*. Fuel Process. Technol. 88 (2007) 1171-1177.
- [2] Lee S., Themelis N.J., Castaldi M.J. *High-temperature corrosion in waste-to-energy boilers*. J. Therm. Spray Technol. 16 (2007) 104-110.
- [3] Persson K., Broström M., Carlsson J., Nordin A., Backman R. *High temperature corrosion in a 65 MW waste to energy plant*. Fuel Process. Technol. 88 (2007), 1178-1182.
- [4] Nielsen H.P., Frandsen F.J., Dam-Johansen K., Baxter L.L. *The implications of chlorine-associated corrosion on the operation of biomass-fired boilers*. Prog. Energy Combust. Sci. 26 (2000) 283-298.
- [5] Salmenoja K., Mäkelä K., Hupa M., Backman R. *Superheater corrosion in environments containing potassium and chlorine*. J. Inst. Energy 69 (1996) 155-162.
- [6] Salmenoja K. *Field and laboratory studies on chlorine-induced superheater corrosion in boilers fired with biofuels*. Doctoral Thesis, Åbo Akademi University, Finland, 2000; Report 00-1.
- [7] Hansen L.A., Nielsen H.P., Frandsen F.J., Dam-Johansen K., Hørlyck S., Karlsson A. *Influence of deposit formation on corrosion at a straw-fired boiler*. Fuel Process. Technol. 64 (2000) 189-209.
- [8] Ma W.C., Rotter S., 2008. *Overview on the chlorine origin of MSW and Cl-originated corrosion during MSW & RDF combustion process*. In: The 2<sup>nd</sup> international conference on bioinformatics and biomedical engineering. Shanghai, China, ICBBE (2008).

## REFERENCES

---

- [9] Krause H.H. *Corrosion by chlorine in waste-fueled boilers*, In: International Conference on Fireside Problems while Incinerating Municipal and Industrial Waste, The Sheraton Palm Coast, Florida, USA, October 8-12, 1989.
- [10] Rademakers P., Hesselings W., van de Wetering, J. *Review on Corrosion in Waste Incinerators, and Possible Effect of Bromine*. TNO Industrial Technology: Apeldoorn, Netherlands, 2002; TNO Report I02/01333/RAD.
- [11] Vehlow J., Mark F.E. *Influence of bromine on metal volatilization in waste combustion*. Journal of Material Cycles and Waste Management 2 (2000) 89-99.
- [12] Vehlow J., Bergfeldt B., Hunsinger H., Seifert H., Mark F.E. *Bromine in waste incineration: Partitioning and influence on metal volatilization*. Environ. Sci. Pollut. Res. Int. 10 (2003) 329-334.
- [13] Bankiewicz D., Vainikka P., Lindberg D., Frantsi A., Silvennoinen J., Yrjas P., Hupa M. *High temperature corrosion of boiler waterwalls induced by chlorides and bromides - Part 2: Lab-scale corrosion tests and thermodynamic equilibrium modeling of ash and gaseous species*. Fuel 94 (2012) 240-250.
- [14] Vainikka P., Enestam S., Silvennoinen J., Taipale R., Yrjas P., Frantsi A., Hannula J., Hupa M. *Bromine as an ash forming element in a fluidised bed boiler combusting solid recovered fuel*. Fuel 90 (2011a) 1101-1112.
- [15] Vainikka P., Bankiewicz D., Frantsi A., Silvennoinen J., Hannula J., Yrjas P., Hupa M. *High temperature corrosion of boiler waterwalls induced by chlorides and bromides. Part 1: Occurrence of the corrosive ash forming elements in a fluidised bed boiler co-firing solid recovered fuel*. Fuel 90 (2011b) 2055-2063.
- [16] Vainikka P., Hupa M. *Review on bromine in solid fuels - Part 2: Anthropogenic occurrence*. Fuel 94 (2012) 34-51.

## REFERENCES

---

- [17] Belevi H., Moench H. *Factors determining the element behavior in municipal solid waste incinerators. 1. Field studies*. Environmental Science and Technology 34 (2000) 2501-2506.
- [18] Huber S., Moe M.K., Schmidbauer N., Hansen G.H., Herzke D. *Emissions from Incineration of Fluoropolymer Materials - A Literature Survey*. Norwegian Institute for Air Research: Kjeller, Norway (2009) ISBN 978-82-425-2085-2.
- [19] Alakangas E., Flyktman M. *Biomass CHP technologies*. VTT Energy Reports 7/2001. VTT Energy, Jyväskylä, Finland. ISSN 1457-3350.
- [20] Basu P. *Combustion and gasification in fluidized beds*. Publisher: CRC Press, Taylor & Francis Group, LLC. (2006) ISBN 0-8493-3396-2.
- [21] Sippula O. *Fine particle formation and emissions in biomass combustion*. Doctoral thesis, University of Eastern Finland, Kuopio Finland (2010).
- [22] Valmari T. *Potassium behaviour during combustion of wood in circulating fluidised bed power plants*. Doctoral Thesis, VTT publications 414, Espoo, Finland, 2000. ISBN 951-38-5569-4.
- [23] Van Loo S., Koppejan J. *The handbook of biomass combustion and co-firing*. London, Sterling, VA. Publisher: Earthscan. (2008). ISBN 978-1-84407-249-1.
- [24] Frandsen F.J. *Ash Formation, Deposition and Corrosion When Utilizing Straw for Heat and Power Production*. Doctoral thesis. Technical University of Denmark, 2011. ISBN 978-87-92481-40-5.
- [25] The European parliament and the council of the European Union. *Directive 2008/98/EC of the European Parliament and of the Council of 19 November 2008 on waste and repealing certain Directives*. Official Journal of the European Union 51 (2008) 3-30.

## REFERENCES

---

- [26] The European parliament and the council of the European Union. *Directive 2002/96/EC of the European Parliament and of the Council of 27 January 2003 on waste electrical and electronic equipment (WEEE)*. Official Journal of the European Union (2002) 24-38.
- [27] The European parliament and the council of the European Union. *Directive 2000/76/EC of the European Parliament and of the Council of 4 December 2000 on the incineration of waste*. Official Journal of the European Union (2000) 91-111.
- [28] Vainikka P. *Occurrence of bromine in fluidized bed combustion of solid recovered fuel*. Doctoral thesis (Åbo Akademi University), VTT publications 778, Finland, 2011c. ISBN 978-951-38-7765-1.
- [29] Kloek W., Jordan K. *Waste generated and treated in Europe - Data 1995-2003*. Luxembourg: Office for Official Publications of the European Communities, 2005. ISBN 92-894-9996-6.
- [30] CEN/TC 343. *CEN/TS 15359:2006 solid recovered fuels – Specifications and classes*. The European Committee for standardization (CEN) 2006.
- [31] CEN/TC 343. *Solid recovered fuels*. The European Committee for standardization (CEN) 2010.
- [32] Gendebien A., Leavens A., Blackmore K., et al. *Refuse derived fuel, current practice and perspectives*. Report no CO 5087-4. UK: European Commission – DG Environment, 2003.
- [33] Cheremisinoff N.P. *Handbook of solid waste management and waste minimization technologies*. (2002), 496 pp. Publisher: (Elsevier Science, New York, N. Y.) ISBN 0-750-67507-1.
- [34] Dunnu G., Maier J., Gerhardt A. *Thermal utilization of solid recovered fuels in pulverized coal power plants and industrial furnaces as part of an integrated waste management concept*. pp 83-91. Book: Appropriate technologies for environmental protection in the developing world.

## REFERENCES

---

Selected papers from ERTEP 2007, July 17–19 2007, Ghana, Africa. Publisher: Springer Netherlands. Editors: Ernest K. Yanful. 2009.

[35] Vehlow J., Hunsinger H. *Municipal solid waste – Generation and composition*, UPSWING Unification of power plant and solid waste incineration, 2005.

[36] Pulkkinen S., Vehmas A., Herkkola H., Sinisalo S. *Pääkaupunkiseudun kotitalouksien sekajätteen määrä ja laatu vuonna 2007*. Helsinki: YTV Pääkaupunkiseudun yhteistyövaltuuskunta, 2008. In Finnish.

[37] Agency for Toxic Substances and Disease Registry (ATSDR). *Public Health Statement Fluorides*. Public Health Service, U.S. Department of Health and Human Services: Atlanta, GA, 2003. [Internet]. <http://www.atsdr.cdc.gov/toxprofiles/tp11-c1-b.pdf> [accessed 06.06.2014].

[38] Çetin Ş., Veli S., Ayberk S. *An investigation of halogens in Izmit hazardous and clinical waste incinerator*. Waste Management 24 (2004) 183-191.

[39] Werkelin J. *Ash-forming elements and their chemical forms in woody biomass fuels*. Doctoral thesis, Åbo Akademi University, Turku, Finland (2008). ISBN 978-952-12-2125-5.

[40] Reid W.T. *The relation of mineral composition to slagging, fouling and erosion during and after combustion*. Progress in Energy and Combustion Science 10 (1984) 159-169.

[41] Zevenhoven M. *Ash-forming matter in biomass fuels*. Doctoral thesis, Åbo Akademi University, Turku, Finland (2001). ISBN 952-12-0813-9.

[42] Zevenhoven R., Kilpinen P. *Control of pollutants in flue gases and fuel gases. Chapter 7. Halogens, dioxins/furans*. (2001) ISBN 951-22-5527-8. [Internet]. [www.abo.fi/~rzevenho/halodiox.PDF](http://www.abo.fi/~rzevenho/halodiox.PDF) [accessed 07.12.2015].

[43] Grabke H.J., Reese E., Spiegel M. *The effects of chlorides, hydrogen chloride, and sulfur dioxide in the oxidation of steels below deposits*. Corros. Sci. 37 (1995) 1023-1043.

## REFERENCES

---

- [44] Pettersson J., Asteman H., Svensson J.E., Johansson L.G. *KCl Induced Corrosion of a 304-type Austenitic Stainless Steel at 600 °C; the Role of Potassium*. Oxid. Met. 64 (2005) 23-41.
- [45] Zhuang Y., Chen C., Timpe R., Pavlish J. *Investigations on bromine corrosion associated with mercury control technologies in coal flue gas*. Fuel 88 (2009) 1692-1697.
- [46] Lai G.Y. *High-Temperature Corrosion of Engineering Alloys*. ASM International: Materials Park, OH, 1990.
- [47] Othman N.K., Othman N., Zhang J., Young D.J. *Effects of water vapour on isothermal oxidation of chromia-forming alloys in Ar/O<sub>2</sub> and Ar/H<sub>2</sub> atmospheres*. Corros. Sci. 51 (2009) 3039-3049.
- [48] Asteman H., Svensson J.E., Johansson L.G., Norell M. *Indication of chromium oxide hydroxide evaporation during oxidation of 304L at 873 K in the presence of 10% water vapor*. Oxid. Met. 52 (1999) 95-111.
- [49] Asteman H., Svensson J.E., Johansson L.G. *Evidence for chromium evaporation influencing the oxidation of 304L: the effect of temperature and flow rate*. Oxid. Met. 57 (2002) 193-216.
- [50] Lehmusto J., Yrjas P., Skrifvars B.J., Hupa M. *High temperature corrosion of superheater steels by KCl and K<sub>2</sub>CO<sub>3</sub> under dry and wet conditions*. Fuel Process. Technol. 104 (2012) 253-264.
- [51] Lehmusto J., Skrifvars B.J., Yrjas P., Hupa M. *Comparison of potassium chloride and potassium carbonate with respect to their tendency to cause high temperature corrosion of stainless 304L steel*. Fuel Process. Technol. 105 (2013) 98-105.
- [52] Kassman H., Bäfver L., Åmand L. *The importance of SO<sub>2</sub> and SO<sub>3</sub> for sulphation of gaseous KCl - An experimental investigation in a biomass fired CFB boiler*. Combustion & Flame 157 (2010) 1649-1657.



## REFERENCES

---

- [53] Kassman H., Broström M., Berg M., Åmand L. *Measures to reduce chlorine in deposits: Application in a large-scale circulating fluidised bed boiler firing biomass*. Fuel 90 (2011) 1325-1334.
- [54] Glarborg P. *Hidden interactions - Trace species governing combustion and emissions*. Proceedings of the Combustion Institute 31 (2007) 77-98.
- [55] Iisa K., Lu Y., Salmenoja K. *Sulfation of Potassium Chloride at Combustion Conditions*. Energy & Fuels 13 (1999) 1184-1190.
- [56] Jiménez S., Ballester J. *Formation of alkali sulphate aerosols in biomass combustion*. Fuel 86 (2007) 486-493.
- [57] Glarborg P., Marshall P. *Mechanism and modeling of the formation of gaseous alkali sulfates*. Combustion and Flame 141 (2005) 22-39.
- [58] Aho M., Vainikka P., Taipale R., Yrjas P. *Effective new chemicals to prevent corrosion due to chlorine in power plant superheaters*. Fuel 87 (2008) 647-654.
- [59] Aho M., Yrjas .P, Taipale R., Hupa M., Silvennoinen J. *Reduction of superheater corrosion by co-firing risky biomass with sewage sludge*. Fuel 89 (2010) 2376-2386.
- [60] Khan A.A., Aho M., de Jong W., Vainikka P., Jansens P.J., Spliethoff H. *Scale-up study on combustibility and emission formation with two biomass fuels (B quality wood and pepper plant residue) under BFB conditions*. Biomass & Bioenergy 32 (2008) 1311-1321.
- [61] Epa.gov [Internet]. US. Environmental Protection Agency (EPA). *Method 26: determination of hydrogen halide and halogen emissions from stationary sources (non-isokinetic method)*. <http://www.epa.gov/ttn/emc/promgate/m-26.pdf> [accessed 07.12.2015].
- [62] Silvennoinen J., Hedman M. *Co-firing of agricultural fuels in a full-scale fluidized bed boiler*. Fuel Process. Technol. 105 (2013) 11-19.

## REFERENCES

---

- [63] Dekati.com [Internet]. <http://dekati.com/cms/dlpi> [accessed 07.12.2015].
- [64] Laurén T. *Methods and instruments for characterizing deposit buildup on heat exchangers in combustion plants*. Licentiate thesis. Åbo Akademi, Faculty of Chemical Engineering, Process Chemistry Center, 2007.
- [65] Westén-Karlsson M. *Assessment of a laboratory method for studying high temperature corrosion caused by alkali salts*. Licentiate Thesis, Åbo Akademi University, Åbo, Finland, 2008.
- [66] Skrifvars B.J., Backman R., Hupa M., Salmenoja K., Vakkilainen E. *Corrosion of superheater steel materials under alkali salt deposits. Part 1: The effect of salt deposit composition and temperature*. Corros. Sci. 50 (2008) 1274-1282.
- [67] Bankiewicz D., Yrjas P., Hupa M. *High-temperature corrosion of superheater tube materials exposed to zinc salts*. Energy & Fuels 23 (2009) 3469-3474.
- [68] Bankiewicz D., Enestam S., Yrjas P., Hupa M. *Experimental studies of Zn and Pb induced high temperature corrosion of two commercial boiler steels*. Fuel Process. Technol. 105 (2013) 89-97.
- [69] Christensen K.A., Livbjerg H. *A field study of submicron particles from the combustion of straw*. Aerosol Sci. Technol. 25 (1996) 185-199.
- [70] Enestam S., Bankiewicz D., Tuiremo J., Mäkelä K., Hupa M. *Are NaCl and KCl equally corrosive on superheater materials of steam boilers?* Fuel 104 (2013) 294-306.
- [71] Shinata Y. *Accelerated oxidation rate of chromium induced by sodium chloride*. Oxid. Met. 27 (1987) 315-332.
- [72] Ignat'eva E.O., Bekhtereva E.M., Garkushin I.K., Kondratyuk I.M. *Phase equilibria in the stable tetrahedron NaF-KF-KBr-K<sub>2</sub>CrO<sub>4</sub> of the quaternary mutual system Na,K//F,Br,CrO<sub>4</sub>*. Russ. J. Inorg. Chem. 58 (2013) 468-473.

## REFERENCES

---

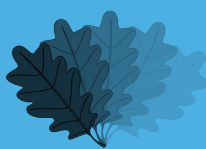
- [73] BSEF. Bromine Science and Environmental Forum. [Internet]. <http://www.bsef.com/our-substances> [accessed 07.12.2015].
- [74] Okoro S.C., Montgomery M., Frandsen F.J., Pantleon K. *Effect of Water Vapor on High-Temperature Corrosion under Conditions Mimicking Biomass Firing*. Energy & Fuels 29 (2015) 5802-5815.
- [75] Wey M.Y., Chen J.C. Wu H.Y., Yu W.J., Tsai T.H. *Formations and controls of HCl and PAHs by different additives during waste incineration*. Fuel 85 (2006) 755-763.
- [76] McNallan M.J., Liang W.W., Kim S.H., Kang C.T. *Acceleration of the high temperature corrosion of metals by chlorine*. High temperature corrosion, Rapp R.A., editor, NACE-6, National Association of Corrosion Engineers, Houston, Texas, USA, 1983, 316-321.
- [77] Lee Y.Y., McNallan M.J. *Ignition of nickel in environments containing oxygen and chlorine*. Metallurg. Trans. 1987,18A,1099-1107.

## RECENT REPORTS FROM THE COMBUSTION AND MATERIALS CHEMISTRY GROUP OF THE JOHAN GADOLIN PROCESS CHEMISTRY CENTRE AT ÅBO AKADEMI UNIVERSITY:

10-01	Markus Engblom	Modeling and Field Observations of Char Bed Processes in Black Liquor Recovery Boilers
11-01	Leena Varila et al.	Fyrtio År Oorganisk Kemi vid Åbo Akademi
11-02	Johan Lindholm	On Experimental Techniques for Testing Flame Retardants in Polymers
11-03	Minna Piispanen	Characterization of Functional Coatings on Ceramic Surfaces
11-04	Sonja Enestam	Corrosivity of Hot Flue Gases in the Fluidized Bed Combustion of Recovered Waste Wood
12-01	Xiaoju Wang	Enzyme Electrode Configurations: for Application in Biofuel Cells
12-02	Patrycja Piotrowska	Combustion Properties of Biomass Residues Rich in Phosphorus
12-03	Dorota Bankiewicz	Corrosion Behavior of Boiler Tube Materials during Combustion of Fuels Containing Zn and Pb
12-04	Mikael Bergelin, Jan-Erik Eriksson, Xiaoju Wang, Max Johansson, et al.	Printed Enzymatic Power Source with Embedded Capacitor on Next Generation Devices, Tekes-PEPSecond
12-05	Susanne Fagerlund	Understanding the in vitro dissolution rate of glasses with respect to future clinical applications
13-01	Oskar Karlström	Oxidation rates of carbon and nitrogen in char residues from solid fuels
13-02	Juho Lehmusto	The Role of Potassium in the Corrosion of Superheater Materials in Boilers Firing Biomass
13-03	Bingzhi Li	Modeling of Fireside Deposit Formation in Two Industrial Furnaces
13-04	Frida Jones	Characterisation of Waste for Combustion –with Special Reference to the Role of Zinc

**RECENT REPORTS FROM THE COMBUSTION AND MATERIALS CHEMISTRY GROUP OF  
THE JOHAN GADOLIN PROCESS CHEMISTRY CENTRE AT ÅBO AKADEMI UNIVERSITY:**

- 14-01 Emil Vainio Fate of Fuel-Bound Nitrogen and Sulfur in Biomass-Fired Industrial Boilers
- 14-02 Niklas Vähä-Savo Behavior of Black Liquor Nitrogen in Combustion – Formation of Cyanate
- 15-01 David Agar The Feasibility of Torrefaction for the Co-firing of Wood in Pulverised-fuel Boilers
- 16-01 Tooran Khazraie Shoulaifar Chemical Changes in Biomass during Torrefaction



Johan Gadolin  
Process Chemistry Centre

ISSN 2343-2535  
ISBN 978-952-12-3400-2 (printed edition)  
ISBN 978-952-12-3401-9 (digital edition)  
Painosalama Oy  
Åbo, Finland, 2016